Identification of a pharmaceutical biostasis inducer that slows metabolism in multiple vertebrates that do not hibernate

Megan M. Sperry[1,2], Berenice Charrez[1], Haleh Fotowat[1], Erica Gardner[1], Kanoelani Pilobello[1], Zohreh Izadifar[1], Tiffany Lin[1], Abigail Kuelker[1], Sahith Kaki[1], Michael Lewandowski[1], Shanda Lightbown[1], Ramses Martinez[1], Susan Marquez[1], Adama M. Sesay[1], Kostyantyn Shcherbina[1], Takako Takeda[1], Kristina Andrijauskaite[3], Exal Cisneros[3], Riley Lopez[3], Isabella Cano[3], Zachary Maxwell[3], Rafael J. Veraza[3], Leon Bunegin[3], Thomas J. Percival[4], Jaclyn Yracheta[4], Jorge Pena[4], Diandra Wood[4], Zachary Homas[4], Cody Hinshaw[4], Jen Cox-Hinshaw[4], Olivia G. Parry[4], Justin J. Sleeter[4], Erik K. Weitzel[4], Michael Levin[1,2,5], Michael Super[1], Richard Novak[1], Donald E. Ingber[1,6,7]*

[1]Wyss Institute for Biologically Inspired Engineering at Harvard University
[2]Department of Biology, Tufts University
[3]Vascular Perfusion Solutions, Inc
[4]RESTOR™, 59th Medical Wing, JBSA, Lackland AFB
[5]Allen Center, Tufts University
[6]Vascular Biology Program & Department of Surgery, Boston Children's Hospital and Harvard Medical School
[7]Harvard John A. Paulson School of Engineering and Applied Sciences
*Corresponding author: Donald E. Ingber, MD, PhD, Wyss Institute at Harvard University, CLSB5, 3 Blackfan Circle, Boston, MA, 02115 USA (Em: don.ingber@wyss.harvard.edu)

ABSTRACT

An injectable 'biostasis' drug that could slow organ injury by inducing a state of suspended animation through reversible slowing of metabolic processes would have great value for organ preservation and treatment of badly injured patients at the point-of-care. Using whole-organism screening of metabolism, mobility, and development in

***Xenopus*, we identified an existing drug, SNC80, that rapidly and reversibly slows biochemical and metabolic activities while preserving cell and tissue viability, independently of its known delta opioid receptor modulating activity. Metabolic suppression was also achieved using SNC80 in cultured cells and microfluidic human organs-on-chips, as well as in explanted whole porcine hearts and limbs, demonstrating the cross-species relevance of this approach and potential clinical relevance for surgical transplantation. Thermal proteome profiling revealed that SNC80 targets the NCX1/EEAT1 membrane transport system and chemical modulation of NCX1 induces biostasis in non-hibernating *Xenopus* tadpoles. Molecular induction of biostasis may offer a new therapeutic approach for organ preservation, trauma management, and enhancing patient survival in remote and low-resource locations.**

Tissue and organ loss to trauma, disease, and physical injury account for a large proportion of human ailments and approximately $400 billion in annual medical burden.[1] The slowing of biological activities or 'biostasis' can buy time for trauma and transplant patients, reduce damage from toxins and overdoses, and improve survival of cells and organs for transplantation. This is currently accomplished clinically by lowering temperature and static cold storage is the standard of care for organ and tissue preservation; however, its long-term use can cause damage to the integrity of the graft.[1–3] Hypothermia also has been used to induce a state of biostasis clinically using *ex-vivo* machine perfusion technologies, for example, during cardiac transplant surgery. Combination of protective agents with perfusion and/or partial freezing approaches have extended preservation times in rat livers and whole pigs,[4,5] and neural modulation approaches have been successful at demonstrating central control of body temperature and general metabolic state.[6,7] However, both mechanical cooling and neural stimulation approaches are challenging to implement in a trauma triage or resource-limited situations, which would be better addressed by pharmaceutical interventions.

Several molecular strategies have been proposed to achieve metabolic suppression for organ preservation, including modulating H_2S, AMPK, opioid receptors, microRNAs, HO-1, and Nrf2.[8] H_2S exposure has been reported to induce a hypometabolic state (reduced metabolism and body temperature) in a rodent model, although this was later found to be mediated in part by a low baseline laboratory temperature.[9] The synthetic opioid peptide DADLE also can induce hypometabolism and improve organ preservation via a delta opioid receptor (DOR) mechanism, but with varied results.[10,11]

Despite these efforts, there remains a large unmet need for improved tissue and organ preservation approaches across multiple application areas. Thus, in the present study, we set out to identify small molecules that could slow metabolism and mimic states normally induced by hypothermia, hibernation, or torpor, which could be used for preservation of living cells, tissues, and organs ex v*ivo*, and potentially *in vivo* as well. A new class of biostasis inducers or 'biostatics' also could have great clinical value for military operations and space exploration, in addition to civilian settings. The major problem we faced, however, is how to approach this monumental challenge without a known human hibernation mechanism or drug target as a starting point.

Through survey of the literature, we identified drugs with unintended side effects, such as lowering body temperature, which suggested they might have broad effects on metabolism. Among these drugs was SNC80, a small molecule drug originally developed as a nonaddictive pain reliever that acts independently of the mu-opioid pathway.[12] This drug caught our attention because it has been shown to induce hypothermia and protect against the effects of spinal cord ischemia in rodents.[12,13] To explore whether SNC80 had potential biostasis-inducing activity, we administered the drug to *Xenopus laevis* embryos and tadpoles, which we and others have previously shown to be useful models for drug screening due to their small size, extrauterine development, and skin permeability to small molecules.[14–17]

Demonstration of stasis induction in *Xenopus*

We first assessed SNC80's impacts on mobility, metabolism, and heart activity in *Xenopus*. Behavioral assessment in mobile tadpoles showed that 100 μM SNC80 slows movement relative to vehicle-treated counterparts, reducing activity by approximately 50% within 1 hour, which is rapidly reversible when the drug is removed (**Figure 1a**). SNC80 also suppressed the rate of oxygen consumption to one-third of baseline (**Figure 1b**) and slowed heart rate to less than half that in controls (**Figure 1c**) within 3 hours of treatment**.** Oxygen consumption was reduced in immobile *Xenopus* embryos treated with SNC80 as well (**Figure S1a**), suggesting that its metabolism-suppressing effects are independent of the slowed movement observed in mobile tadpoles.

Using *in situ* Matrix-Assisted-Laser Desorption/Ionization-Time of Flight Mass Spectrometry Imaging (MALDI-ToF MSI), we assessed and visualized the biodistribution of SNC80 in the *Xenopus* tadpole. SNC80 was detected within 1 hour of treatment and it appeared in a punctate distribution in the gastrointestinal (GI) tract, gill region and skeletal muscle (**Figures 1d** & **S1b,c**), suggesting full-body delivery of the drug.

Past lipidomic studies of hibernating mammals demonstrated the importance of lipid molecules for thermal adaptation during hibernation with significant alterations of lipidomic profiles being observed in liver, plasma, brain, skeletal muscle and cardiac muscle during torpor as compared to the animal's active state.[18,19] Similarly, MALDI-ToF MSI analysis revealed significantly higher levels of acylcarnitine and cholesterol ester in SNC80-treated groups in both skeletal muscle and brain (**Figure S1d**). Increased levels of long chain acylcarnitine associated with enhanced mitochondrial fatty acid oxidation are observed during fasting as well as in hibernating brown bears,[20,21] and cholesterol ester levels increase in hibernating ground squirrels.[22] While the increased acylcarnitine and cholesterol ester levels in brain suggest a shift towards beta oxidation of fatty acids, they also have been implicated in other pathways including antioxidant activity and neurotransmission.[23,24]

Having confirmed that SNC80 induces a state of biostasis in the whole *Xenopus* organism, we then set out to identify the molecular basis for these effects. As SNC80 is a known DOR agonist,[12,13] we next evaluated whether its biostasis effects could be mediated by delta opioids. However, when we tested the DOR antagonist, naltrindole (NTI), at concentrations up to 200 μM, it did not block the stasis-inducing effects of SNC80 (**Figure 1e**), suggesting that SNC80 modulates metabolism independent of DOR activation.

Stasis induction in cultured human cells and tissues

To explore whether this drug also induces a state of biostasis in cells and tissues of higher organisms, we tested SNC80 in multiple types of cultured human cells as well as in human organ-on-a-chip (Organ Chip) microfluidic culture devices that reconstitute tissue-tissue interfaces and human organ-level physiology with high fidelity in vitro.[25] We monitored the effects of SNC80 on oxygen consumption in four different types of cultured human cells — human umbilical vein endothelial cells (HUVEC), Caco-2 intestinal epithelial cells, liver sinusoidal endothelial cells (LSEC), and Huh7 liver epithelial cells — and analyzed multiple indicators of cellular metabolism, including mitochondrial respiration using the oxygen consumption rate (OCR) and ATP production.

Treatment with SNC80 (100 μM) suppressed oxygen consumption relative to control levels within 1.5 hours in epithelial cells derived from intestine and liver (**Figure 2a**) without detectable cytotoxicity (**Figure S2a**), indicating a decrease in cellular metabolism similar to *Xenopus*. While SNC80 treatment did not alter oxygen consumption rate (OCR) in either of the endothelial cells (HUVEC or LSEC), it reduced mitochondrial ATP production in the intestinal epithelial cells and both endothelial cell types (**Figure 2a**), indicating a decrease in mitochondrial activity and slowing of metabolism. Furthermore, we observed a reduction in creatine kinase activity in both epithelial cell types (**Figure S2b**) indicating a decrease in overall cell energy demand.[26]

However, cells also can compensate for decreased mitochondrial ATP production by activating other metabolic pathways.[27–29] To assess this, we measured the extracellular acidification rate (ECAR), an indicator of lactic acid production due to glycolytic activity, as well as glutamate, and found an increase in glutamate production by Caco-2 cells exposed to SNC80 (**Figure S2b**), while in other cell types, the ECAR and glutamate production remained unchanged with SNC80 treatment (**Figure S2b**). SNC80 must therefore decrease total ATP production, which was confirmed by detection of a significant drop in the ATP/ADP ratio within liver epithelial cells expressing a fluorescent reporter (**Figure 2b and Figure S2c**). Taken together, these results indicate that all four human cell types showed significant decreases in mitochondrial metabolism in response to the biostasis inducer SNC80. However, some cells activated compensatory pathways in response to the impaired mitochondrial respiration, while others just allowed for their energy balance to decrease significantly.

We then extended these studies to test the effects of SNC80 in more physiologically relevant human Organ Chip models that reconstitute a tissue-tissue interface between organ-specific epithelium and endothelium across a porous extracellular matrix-coated membrane within a two-channel microfluidic device, as previously described.[30,31] In this study, we used a Gut Chip lined by Caco-2 intestinal epithelial cells interfaced with HUVECs and a Liver Chip containing Huh7 liver epithelial cells interfaced with LSECs, respectively. However, we modified the Organ Chip design by integrating sensors that allow for live monitoring of oxygen (O_2) and transepithelial electrical resistance (TEER) (tissue barrier function) (**Figure S3a**). Both Organ Chips were treated with SNC80 by flowing the drug in medium for 2 days through the apical and basal channels of the chip, and then removing the drug followed by 7 days of additional culture. We confirmed that the epithelial cells underwent villus differentiation and accumulated mucus under these culture conditions (**Figure S3b**) as well as a low oxygen environment after 10-16 days of culture (**Figure S3c**) as previously described.[30,31] The Liver Chips also maintained

production of albumin and urea at levels (5 and 135 μg/day/chip, respectively) (**Figure S3d,e**) that were similar to those measured in Organ Chips lined by primary hepatocytes.[32,33]

These studies revealed that SNC80 treatment reduced the respiratory (oxygen utilization) rate in the Gut Chip, resulting in an almost 6-fold increase in extracellular oxygen levels after 48 hours, which then progressively returned to baseline levels during the 7-day washout period (**Figure 2c**). Similar results were obtained with the more highly metabolic Liver Chip with SNC80 inducing higher levels of extracellular oxygen compared to control chips and this again reversed after drug washout (**Figure 2c**). Importantly, the tissues in both the human Organ Chips remained healthy after 2 days treatment with SNC80 as there was no significant change in barrier function (**Figures S4a,b**), cell growth (**Figure S3**), or cytotoxicity (**Figures S4c,d**). Similar to the data observed in cell cultures, ATP/ADP ratio in Liver Chips was significantly decreased over 24 and 48h of SNC80 treatment compared to the vehicle control Chips. However, ATP/ADP ratio measurements between SNC80 and vehicle control were not significantly different after washout of the drug, indicating that Liver Chip tissues recover their normal metabolic function up to 4 days after treatment (**Figure 2d**).

Collectively, these data suggest that this biostasis induction resulted from a drop in mitochondrial respiration given that mitochondria make up for 70%–90% of total oxygen consumption.[34] Moreover, there was no switch towards glycolysis or reductive carboxylation in these more physiologically relevant Organ Chip systems as the levels of lactate (**Figure S4e,f**) and glutamate remained unchanged in both chips (**Figure S4g,h**). Thus, in this organ-like microenvironment, the tissues decrease their total ATP production in presence of SNC80, which is accompanied by a global slowing of metabolism.

Biostasis induction in whole pig organs perfused *ex vivo*

Based on these intriguing findings with cultured cells, we set out to explore the potential clinical value of this biostasis inducer drug. Cardiac transplant is the gold standard for treating end-stage heart failure; however, it is hindered by the donor shortage, limited cardiac graft

preservation time, and lack of optimal organ preservation conditions. To explore the potential utility of biostasis induction for this application, we perfused surgically explanted whole porcine hearts with SNC80 using a portable, oxygenated perfusion preservation device (VP.S ENCORE®) at subnormothermic temperatures (20-23°C). The hearts were perfused for 3 hours with oxygenated buffer after cannulation before SNC80 or vehicle control was injected through the arterial line and perfused for a total of 8 hours. While there were no changes in heart metabolism during the first 3-hour drug-free period, the relative metabolic rate reduced in SNC80-treated hearts compared to vehicle controls during the subsequent 5-hour perfusion (**Figure 3a**).

After preservation, hearts were removed from the VP.S ENCORE® and placed in a Langendorff system for reperfusion and evaluation of oxygen consumption and cardiac contractility. After 30 minutes of reperfusion and before defibrillation, SNC80-treated hearts had a lower oxygen consumption level than vehicle treated hearts (1.64 ± 0.29 versus 3.91 ± 1.62 ml/min/100g, respectively, at the 30-minute timepoint) (**Figure 3b)** that recovered to normal levels after defibrillation and with increases in temperature (2.95 ± 0.54 and 3.76 ± 0.63 ml/min/100g, respectively, averaged over 40 minutes post-defibrillation) (**Figure 3c**). No evidence of change in left ventricle (LV) contractility was detected in SNC80-exposed hearts, either before or after they were defibrillated and exposed to epinephrine (**Figure 3d**). Most importantly, gene expression analysis of heart biopsy samples showed significant reduction of markers of inflammation (IL-6, TNFα), hypoxia (Hif1α), and cell death (TP53) in SNC80-treated hearts when compared to vehicle control hearts (**Figure 3e**).

We also tested a similar preservation approach in porcine limbs where prolonged ischemia after amputation rapidly decreases the viability of skeletal muscle. Current preservation methods limit the success of limb reimplantation due to complications from rhabdomyolysis, necrosis, and reperfusion injury.[35] Again, we found that the relative metabolic rate measured during 3 hours of SNC80 exposure was significantly lower compared to vehicle-

treated limbs (**Figure S5a**). Histopathological evaluation showed retention of normal muscle morphology with no apparent changes in muscle bundle area (**Figure S5b**) or glycogen content (**Figure S5c**) suggesting that the tissue's potential for ATP synthesis was not compromised after SNC80 administration, although an increase in intercellular spacing was observed (**Figure S5d**). We did not observe recovery of O_2 uptake at the 3-hour time point analyzed in this study (**Figure S5c**); however, the porcine limb contains a large amount of fat tissue that may be acting as a depot for the highly lipophilic SNC80, thereby leading to extended stasis under these conditions.

Elucidating the biostasis induction mechanism

To gain insight into the molecular basis of biostasis induction, we used thermal proteome profiling (TPP) to assess drug-protein binding and thereby identify previously unknown molecular targets of SNC80 that might be critical for its metabolism slowing activity. TPP of SNC80-treated *Xenopus* tissues revealed that EAAT1 is a direct binding target of SNC80 and that the related transporter Na^+/Ca^{2+} exchanger 1 (NCX1; also known as SLC8A1) is an indirect target (**Figure 4a**). Interestingly, mitochondrial ATP production has been previously reported to be stimulated through intermolecular interactions between EAATs and NCXs,[36] and thus, inhibition of EAAT and NCX1 would be expected to reduce cellular ATP levels.[37] We also identified other direct and indirect targets of SNC80, including multiple targets involved in transmembrane transport, mitochondrion activity, and metabolic processes (**Table S1**), which could further contribute to biostasis-inducing activity. However, these findings suggest that binding of SNC80 to EAAT1 may modulate EAAT1-NCX1 interactions on the mitochondrial membrane and thereby play a central role in slowing metabolism by blocking ATP production.

To directly assess the role of EAATs and NCXs in stasis induction, we treated *Xenopus* tadpoles with specific inhibitors of these channels. Interestingly, treatment with a high concentration (500 μM) of the EAAT inhibitor, DL-TBOA, for 5 hrs did not slow tadpole movement (**Figure 4b**) or alter oxygen consumption (**Figure 4c**), suggesting that direct

blockade of EAAT alone is not sufficient to slow *Xenopus* metabolism. In contrast, treatment with the NCX1 blocker, aprindine, significantly reduced both swimming activity (**Figure 4b**) and oxygen consumption (**Figure 4c**). The outcomes of aprindine are similar to the effects observed with SNC80, including recovery of swimming behaviors after treatment washout. We also tested two other NCX blockers (KBR-7943 and dronedarone) which similarly reduced swimming (**Figure S6**); however, inconsistent recovery was observed after treatment, suggesting potential toxicities or irreversibility of the stasis mechanism using these compounds. Moreover, inhibition of NCX using aprindine also decreased mitochondrial respiration in LSECs (**Figure S7a**) and suppressed mitochondrial ATP production in all four human cell types tested (**Figure S7a,b**).

These results are consistent with a mechanism whereby SNC80 directly binds EAAT1 without altering its activity, however, it may interfere with interactions between EAAT1 and NCX1 that are critical for transmembrane signaling and resultant ATP production in the mitochondrion (**Figure 4d**). Specifically, the blockade of Na^+/Ca^{2+} exchange via interference with EAAT1-NCX1 interactions could prevent the influx of calcium into the mitochondria that is necessary for calcium-sensitive mitochondrial dehydrogenases that fuel ATP synthesis.[38]

Discussion

Here we report the discovery that the small molecule drug, SNC80, is capable of inducing a hypometabolic state of biostasis without external cooling. Although there is extensive clinical experience using hypothermia to cryopreserve organs during surgery (e.g., cardiac bypass) and for donor transplants, comparatively little work has been done in the area of molecular induction of biostasis without external cooling. We found that SNC80 reversibly suppressed metabolism across multiple cell and tissue types, as well as different species and experimental models, at their basal temperatures, suggesting that this approach could be appropriate for preservation of a variety of cells, tissues, and organs. Critically, integrating this molecular biostasis inducer in a commercial organ preservation system with whole explanted

pig hearts demonstrated potential for near-term translation and impact of this approach on organ donation and surgical transplantation.

Initially developed as a nonaddictive pain reliever, SNC80 was previously shown to induce hypothermia and protect against the effects of spinal cord ischemia in rodents,[12,13] but its broad effects on metabolism were not known. In the present study, treatment with SNC80 slowed swimming movement and reduced oxygen consumption rates in a reversible manner in *Xenopus* tadpoles, and it lowered the metabolic rate in non-mobile *Xenopus* embryos as well. Importantly, SNC80 displayed similar metabolism suppressing activities that were reversible in four different types of human cultured cells when cultured individually or within more physiologically relevant human Organ Chip microfluidic devices that reconstitute organ-level structures and functions in vitro. These data suggested that induction of a torpor-like state of suspended animation by this small molecular drug could potentially provide a new paradigm to prolong organ preservation. Indeed, when we perfused explanted porcine hearts and limbs with SNC80, we experimentally confirmed that this biostasis agent can slow metabolism in a whole complex living organs, providing direct support for its potential integration into commercial organ preservation devices that strive to extend the viability of human organs for surgical transplantation.

SNC80 is defined as a highly selective non-peptide DOR agonist drug and other DOR agonists, such as the enkephalin DADLE, have been shown to reduce metabolic demand and protect against oxidative stress, thereby decreasing injury and apoptosis in perfused organs.[8,10,11] Prior studies of DADLE found that the DOR pathway was required to alter metabolism and provide protective effects, however, we found that SNC80 suppresses metabolism via a mechanism that is independent of its DOR modulating activity. Instead, we found that SNC80 interacts with multiple proteins involved in transmembrane transport, mitochondrion activity, and metabolic processes, and we identified the NCX1/EAAT1 complex as a new target for inducing biostasis. Interestingly, a similar NCX1-related mechanism has

been previously implicated in control of temperature compensation and autonomous oscillation,[39] suggesting that it plays a key role in the regulation of biochemical reaction speed, cell cycle, and other forms of biological timing, such as circadian rhythm. However, given the high potential for impacting tissues of the central nervous system with SNC80 treatment, future work should focus on further characterizing cognitive recovery in organisms receiving systemic delivery of stasis inducers.

In addition to its effects on tissues of the nervous system, multiple drugs that target Na^+/Ca^{2+} exchange by NCX, such as the KBR family of drugs, were developed for the treatment of ischemia, reperfusion injury, and heart arrhythmias.[40] In rats, pre-ischemic or post-ischemic treatments with KBR compounds improved recovery of ventricular pump function and reduced reoxygenation-induced injury as measured the reduced release of intracellular components (e.g., lactate dehydrogenase).[40,41] Our results suggest that the tissue-protective effects obtained by modulating the NCX1 transmembrane protein and/or NCX1/EAAT1 pathway may result at least in part from induction of a hypometabolic state of biostasis. Interestingly, our studies with cultured human cells suggest that the metabolism-suppressing effects of SNC80 were most potent in the Caco2 and Huh7 cell lines that were originally derived from more highly metabolic tumors, which is also consistent with past work suggesting that targeting of the NCX1 channel might offer a way to slow cancer growth.[42]

In summary, our findings demonstrate that a small molecule drug can be used to induce a state of biostasis similar to that normally induced by cooling, and demonstrate the therapeutic potential of this type of biostasis inducer for clinical applications, such as enhanced preservation of organs. The use of a biostatic compound in combination with a self-contained transport system could potentially increase organ viability for sustained times *ex vivo*, thus helping to advance organ and tissue preservation for surgical transplantation. The ability to induce a reversable hypometabolic, suspended animation-type state rapidly through injection at the point-of-care also could enable new therapeutic approaches to slow the detrimental effects of trauma

and acute infection, thereby increasing patient survival in military settings and space exploration, as well as in civilian health emergency operations. It also may be possible to use this biostasis approach to slow metabolic activities in the brain in cases of stroke or traumatic brain injury, indications for which current treatments are severely limited.

Methods

***Xenopus* model.** *Xenopus* embryos were fertilized at Tufts University using procedures reviewed and approved by the Tufts University Institutional Animal Care and Use Committee regulations and transferred to the Wyss Institute. *Xenopus* embryos and tadpoles were housed at 18°C with a 12/12 h light/dark cycle in 0.1X Marc's Modified Ringer's (MMR) medium. All animal experiments and procedures were reviewed and approved by the Harvard Medical School (HMS) Institutional Animal Care and Use Committee regulations.

Drugs used in the *Xenopus* studies were dissolved in DMSO to a stock concentration of 10 mM and diluted to their final concentrations with a 1% DMSO concentration or less (drug doses and sources are described in **Table S2**). Media with dosed compound were made fresh and screening was performed in tadpoles at Stages 46-50. The activity of free-swimming tadpoles during and after exposure to drugs were recorded in 60 mm dishes or 24-well plates using a SONY Alpha a6100 camera with 16 mm objective (Sony Corporation, Tokyo, Japan) against an illuminated background. Mobility was quantified in Matlab (Mathworks, Natick, MA) by mapping differences between frames to a movement index (0 – 1), with 0 indicating no movement and 1 indicating maximal movement. Oxygen consumption was measured during *Xenopus* exposure to drugs as a proxy for whole-organism metabolism using the Firesting Optical Oxygen Meter and the Pyro Oxygen Logger software (version 3.317) (Pyroscience GmbH, Aachen, Germany). Oxygen consumption rate for each sample was measured using a linear fit to the oxygen consumption over 3 hours of data in Prism (GraphPad, San Diego, CA). Heart rate was measured by microscopy imaging in *Xenopus* following 1 hour of drug exposure. Vehicle and drug-treated groups were briefly incubated in 0.01% tricaine (Syndel, Ferndale, WA) to minimize tadpole movement during heart imaging. Videos of heart function were acquired using a ZEISS Axio Zoom.V16 microscope and ZEN BLUE Microscopy software (version 3.1) (Carl Zeiss AG, Oberkochen, Germany) at a rate of 1 frame/100 ms. Heart beats

were counted automatically in Matlab by mapping differences between video frames to a movement index and identifying local maxima in the movement index. Automated counting was previously validated by comparison of Matlab outputs with manual counting by two independent assessors. At the completion of experiments, *Xenopus* were euthanized by immersion in 0.2% tricaine for 30 minutes, followed by fixation or bleaching and disposal.

MALDI-ToF. Tadpoles were embedded in gelatin (0.11 g/mL) and stored in -80C. Embedded tadpoles were sectioned into 16 um-thick slices using a Leica CM1850 (Leica Microsystems, Wetzlar, Germany) onto indium tin oxide (ITO)-coated glass slides (Bruker Daltonics, Billerica, MA) and immediately placed in a vacuum desiccator before matrix application (N=5 tadpoles per condition; N=3 sections/slide). Experiments were duplicated to confirm the reproducibility. The matrix solution was composed of 2,4 Dihydroxybenzoic acid (40mg/mL) in 0.1% formic acid, methanol/water (1:1 v/v) and was made fresh for each application. The HTX-sprayer nebulizer (HTX Technologies, Carrboro, NC, USA) was used to apply the matrix at 80°C at 24 passes over the sample, at a flow rate of 50μL/min, 10 psi pressure and a track speed at 1,250 mm/min. Before imaging, SNC80 spotting with matrix and *Xenopus* lysate was performed to determine the optimal matrix for the best S/N ratio and the least ion suppression from *Xenopus* tissue and to identify which adducts were detectable for each compound for imaging. *In situ* MALDI-ToF imaging was acquired using the rapifleX (Bruker Daltonics, Billerica, MA), in positive ion mode at 1000 Hz in the mass range of 300-990 m/z. The laser raster step spacing was set to 45 μm step size at 500 shots per pixel. External calibration was performed using a red phosphorus slurry drop casted on a region of the ITO slide without tissue. Preliminary processing of the data was performed using FlexAnalysis (Bruker Daltonics, Billerica, MA). Images were normalized by the total ion count and baseline-corrected using Top Hat algorithm with a _baseline width. After MALDI-ToF MSI acquisition, ITO slides were then stained for H&E and imaged using the Cytation 5 (Agilent, Santa Clara, CA) and Epsilon scanner at 3000 dpi to select regions of interest using the open-source program, Qupath.[43]

Further data analysis was conducted with SCiLS (Bruker Daltonics, Billerica, MA), where images were generated from the list of target m/z values for SNC80 as well as validated in Xenopus tissues from previous findings[44] within a 0.2 Da range and PCA analysis was used to identify peaks.

Thermal proteome profiling. To identify drug-bound targets based on altered thermal stability, *Xenopus* tadpoles were treated with either SNC80 or vehicle for 2 hours. *Xenopus* were euthanized in 20X tricaine and then transferred back to their respective drug solutions to ensure drug effect is not lost during heat treatment. *Xenopus* samples were incubated at 9 temperature points (30C, 35C, 40C, 44C, 48C, 52C, 56C, 60C, 65C) using a PCR machine (3 minutes heat time per condition, 3 tadpoles per condition) for both drug treated and vehicle treated groups. After transfer to room temperature, liquid was aspirated from samples and samples were snap frozen in liquid nitrogen. Samples were lysed in 100 µl of PBS + 0.4 % NP-40 with 4 cycles of freeze/thaw. 11µl of each of the 9 temperatures were pooled in one tube and samples were centrifuged at 13,000 RPM for 75 minutes, at 4C. Proteins were reduced and alkylated with 10 mM DTT and 15 mM IAA for 15 minutes at 65C and 30 minutes at room temperature, respectively. Proteins were then precipitated with 8 volumes of ice-cold acetone and 1 volume of ice cold methanol overnight. Digestion was carried for 4 hours in 50 mM Tris ph 8 + 0.75 mM Urea + 1µg trypsin/LysC at 37 Celcius with agitation. Another 1 µg of trypsin/LysC was added and digestion was continued overnight. Peptides were purified by reversed phase SPE and analyzed by LC-MS/MS (PhenoSwitch Bioscience, Sherbrooke, QC, Canada). LC-MS/MS acquisition was performed with a ABSciex TripleTOF 6600 (ABSciex, Foster City, CA, USA) equipped with an electrospray interface with a 25 µm iD capillary and coupled to an Eksigent µUHPLC (Eksigent, Redwood City, CA, USA). Analyst TF 1.8 software was used to control the instrument and for data processing and acquisition. Samples were acquired twice in SWATH acquisition mode using gas phase fractionation. The source voltage was set to 5.5 kV and maintained at 325C, curtain gas was set at 45 psi, gas one at 25 psi and gas two at 25 psi.

Separation was performed on a reversed phase Kinetex XB column 0.3 µm i.d., 2.6 µm particles, 150mm long (Phenomenex) which was maintained at 60C. Samples were injected by loop overfilling into a 5µL loop. For the 60 minutes LC gradient, the mobile phase consisted of the following solvent A (0.2% v/v formic acid and 3% DMSO v/v in water) and solvent B (0.2% v/v formic acid and 3% DMSO in EtOH) at a flow rate of 3 µL/min. GPF files for both acquisitions were analyzed on a previously generated 3D ion library. Each GPF file was analyzed using 10 peptides per protein, 4 MS/MS transition per peptide, 12.5-minute RT window and 25 ppm XIC width in Peakview (Sciex). The reported quantification for a protein is the sum of all the correctly integrated peptides (FDR<0.05) in both GPF files.

Human Cell Cultures: Caco2 intestinal epithelial cells were grown in high glucose (4.5g/L) DMEM (Gibco), 10% FBS (Gibco) and 1% penicillin/ streptomycin (Gibco) and subcultured every 2-3 days at 1:6 ratio. For all experiments, cells were used between passage 59 and 64. HUVE cells were maintained in EBM-2 (Lonza) media with EGM-2 BulletKit (Lonza), 2% FBS and 1% penicillin/streptomycin (Gibco) and subcultured every 2-3 days at 1:6 ratio. For all experiments, cells were used between passage 3 and 7. HuH-7 liver epithelial cells were maintained in DMEM with 4.5g/L glucose (HyClone), 10% FBS and 1% penicillin/ streptomycin (Gibco). We also obtained wild-type Huh7 transduced with lentivirus particle pLV[Exp]-Puro-CMV>{Perceval(ns)}:T2A:mCherry/3xNLS (Vector Builder) that were used for live imaging of changes in ATP/ADP ratio within these cells, which directly correlates to cellular metabolic activity.[45] LSEC cells were maintained in EBM-2 (Lonza) media with EGM-2 BulletKit (Lonza), 2% FBS and 1% penicillin/streptomycin (Gibco).

Seahorse assay: The Seahorse Mitostress assay (Agilent) on Agilent XFe24 plate was used to measure mitochondrial metabolism for Caco-2, Huh7, HUVEC, and LSEC cells. Cells were added in all wells except 4 designated wells used for background measurements. Cell concentrations were chosen to be 90% confluent on the day of experiment. Manufacturer's protocol was followed. The drugs concentrations were prepared in Seahorse XF medium at a

10x concentration stock: 1mM SNC80, 500uM Aprindine, 250-1000uM KBR-9743 and 250-1000uM Dronedarone. Baseline OCR and ECAR measurements were taken before the drugs were injected. Drugs were incubated for 2h, before mitochondrial inhibitors were successively injected in the following order: 10uM Oligomycin, 10uM FCCP, 5uM AntimicinA/Rotenone. Agilent Wave software was used to process the data.

Metabolic assays: For cell assays, each cell type (Caco-2, Huh7, HUVEC, LSEC) was plated in 96 well plates and exposed to 100uM SNC80 or 1:100 DMSO vehicle for 2h. After treatment, the effluent was collected and analyzed for lactate and glutamate production using the Lactate-Glo™ (Promega, #J5021) and Glutamate-Glo™ (Promega, #J7021) assay kits respectively as per manufacturer protocols. In the case of Organ Chips, effluents were collected at different timepoints (baseline, 24h, 48h and 1-3 days recovery after washout) throughout the exposure to SNC80 or 1:1000 DMSO vehicle and the same assays were performed.

Cytotoxicity assay: Cytotoxicity measurements on the Organ Chip effluents were performed using the LDH-Glo™ (Promega, #J2380) as per manufacturer protocols. CytoTox-ONE™ assay (Promega, #G7890) was used to assess membrane integrity and cyctotoxicity of plated cells after 2h exposure to 100uM SNC80 or 1:100DMSO vehicle as per manufacturer protocols.

Creatine kinase assay: Creatine Kinase Colorimetric Activity Assay Kit (abcam, #ab155901) was used to measure CK activity in adherent cells (Caco-2, Huh7, HUVEC, LSEC) exposed to 2h SNC80 or 1:100 DMSO vehicle control as per manufacturer's protocol.

ATP/ADP ratio measurements: Huh7 cells were transfected with a reporter that enables direct measurements of cellular ATP:ADP ratio. The basal excitation spectrum of the reporter protein was similar to that of YFP (peak around 490 nm) but it had an additional peak at CFP wavelength (405 nm). As ATP levels decreased, more ADP can bind to the site, decreasing the YFP/CFP ratio value. BioTek Cytation 5 Cell Imager (Agilent) was used to take RFP, YFP and CFP images of each well every 20min for 180 minutes upon exposure to 100uM

SNC80 or 1:100 DMSO vehicle. Post processing of the images was performed using the open source CellProfiler program.[46] We implemented the following pipeline to obtain quantitative ATP/ADP ratio values (see **Figure 2b**): (1) Identify nuclei with RFP marker, (2) Define a cell as 4pixels around the edge of the nuclei, (3) Measure cells YFP and CFP intensity and YFP/CFP ratio, (4) Count cells per Image, (5) Track cells YFP and CFP intensity over timecourse (0-3h with 20min intervals), (6) Measure YFP/CFP ratio average **over all cells** per image and normalize to cell count (7).

For the qualitative images (see **Figure 2b**), raw images were processed with ImageJ by using the image calculator to divide yfp/cfp intensity of respective images. “Rainbow RGB” lookup table was used to show the intensity changes. Tones towards the red show more intensity, higher ATP/ADP ratio and higher metabolism.

Organ Chips with Integrated Sensors: To allow for live oxygen and transepithelial\endothelial resistance (TEER) monitoring, we used our in-house developed and fabricated microfluidic chips with integrated TEER and oxygen sensors. To mimic the in vivo-like cell-cell interface on the models, a dual-channel PDMS microfluidic chip was used where the apical channel is separated from the basal channel with a porous PDMS membrane. A pair of TEER sensing electrodes where integrated on the apical side of the top channel and the basal side of the bottom channel to measure the electrical resistance across the epithelium-endothelium tissue interface. The O_2 sensing nanoparticles (OXNANO, PyroScience) were integrated at four different locations in the chip: two in the apical channel and two in similar locations in the bottom channel. This is to allow a fair representation of the whole chip oxygen tension levels.

After fabrication, the chips were sterilized by plasma treatment and desiccated for 30 minutes. The polymeric surfaces of the membrane were then chemically functionalized using ER1/ER2 buffers following Emulate™ Inc. protocol and coated with extracellular matrix (ECM) for 1.5-2 hours at 37°C. Gut Chip apical and basal channels were coated with 30 µg/ml

Collagen I (Advanced BioMatrix, Cat. no. 5005) and 100 µg/ml Matrigel (BD Biosciences) in cold PBS. Liver Chip apical channel was coated with 30 µg/mL fibronectin (Corning, Cat. no. 356008) and 400 µg/mL Collagen I (Advanced BioMatrix, Cat. no. 5005) in cold DPBS, while the basal channel was coated with 100 µg/mL Matrigel (BD Biosciences) and 200 µg/mL type I collagen in cold DPBS. To create Gut Chip, HUVECs (6-8x10^6 cells/ml (P5)) were first seeded on the bottom side of the permeable membrane in the basal channel and incubated for 2-3 hours at 37°C before seeding the Caco-2 cells (2-3x10^6 cells/ml (P78)) on the membrane in the apical channel. Liver Chip was similarly created by seeding the LSEC (4-5x10^6 cells/ml (P3-8)) the first in the basal channel followed by seeding he Huh7 hepatocytes (2.5-3.5x10^6 cells/ml (P5-15)) on the membrane in the apical channel The chips were then cultured under continuous flow using the commercial culture module instrument (ZOË™ Culture Module, Emulate Inc.,USA). The Gut Chips were maintained under continuous flow of 30µl/hr in the apical and basal channels for 10 days before changing their respective media to differentiation-promoting media (5% FBS in DMED apically and 0.5% FBS endothelial medium basally) for the rest of the culture time. The Liver Chips were also maintained under continuous flow of growth media at 30µl/hr in the apical and basal channels for 5-6 days before reducing the FBS content to 5% in Huh7 media and 0.5% in LSEC media for inducing tissue differentiation.

Human Organ Chip studies: SNC80 was tested on the Gut Chip at day 16 of culture, when the epithelium showed characteristics of matured, functional tissue and the Liver Chip was tested after 7-10 days of culture. SNC80 [100µM] in the culture media was perfused through the apical and basal channels of the chips at 30µl/hr, while the control chips were perfused with the same culture media containing the compound's vehicle [0.5% DMSO] using the same flow condition. The chips were treated with SNC80 for 48 hours before the drug was removed from the media and the culture was continued for another 4 days. Both Liver and Gut Chips were monitored at d-1, 0h, 3h, 24, 48h timepoints as well as day 1 and 3 after the drug washout for oxygen consumption, TEER measurements, and effluent analysis. Fluorescence microscopy

was continuously performed from 0h throughout the treatment period and up to 3 days of recovery. CellProfiler program was used to analyze ATP/ADP ratio as described above.

Oxygen and TEER measurements on-chip: Oxygen tension level measurements was performed on-chip during the culture using FireSting®-O2 Optical Oxygen and Temperature Meter (FSO2-C4, Pyroscience sensor technology, Germany) connected to Pryo Oxygen Logger (V3.317©, Germany). TEER measurements were performed on-chip using our in-house developed multiplexed TEER Tray and remotely measured from outside the incubator. A four-point impedance measurement was taken on-chip periodically every 24 hours during the SNC80 treatment and recovery using the IviumSoft application (V4.97, Informer Technologies, Inc.). To obtain the TEER of only the epithelial-endothelial tissue interface, the measured impedance at 100Hz was subtracted from the impedance at 100kHz and reported as the tissue impedance(Ω) throughout the culture and in response to different stimuli as we reported previously.[47]

DNA damage and proliferation assays: The Click-IT™ EdU cell proliferation kit (Thermofisher, #C10337) was used to assess cell proliferation in the formaldehyde-fixed chips and DNA damage was assessed by staining anti-H2AX antibody (Novus Bio NB100-2280).

Urea Assay: Urea nitrogen was measured using a colorimetric assay (urea nitrogen test, Stanbio Laboratory), whereby undiluted liver chip effluents were added to a 96 well plate and mixed with the kit's working reagents as per manufacturer protocol.

Albumin Assay: Liver albumin production was measured using an enzyme-linked immunosorbent assay (Bethyl Laboratories). Liver Chip effluents were diluted 1:100 in buffer before being plated in the kit's 96 well plate, aside from standard wells with dilution series of known albumin concentration solution. We followed manufacturer protocol to perform the sandwich ELISA assay and measure absorbance at 450nm.

Porcine heart ex vivo perfusion studies: After induction of anesthesia and preparation for clean, non-survival surgery, a median sternotomy was performed followed by longitudinal incision in the pericardium to expose the heart and the great vessels. Following blunt dissection

and exposure of the vena cava, aorta and the brachycephalic artery, the superior vena cava, and azygos vein was ligated and divided. The brachycephalic artery was catheterized for infusion of cardioplegia solution. The inferior vena cava was clamped and divided proximal to the clamp. Two or three pulmonary arteries were incised for decompression of the left side of the heart. The aorta was immediately clamped and 10-15 ml/kg of body weight of cold (2-4°C) cardioplegia solution (del Nido without lidocaine, 3 L) was infused at a pressure of 70-80mmHg to stop the heart. Cold 4°C saline and ice were poured over the heart and the accumulated fluids from the thoracic cavity were removed by suction. Following cessation of myocardial function, the heart was removed from the chest by further dissection and division of the pulmonary vessels and aorta distal to the clamp. The heart was cooled in a surgical bowl with cold saline for inspection and preparation for perfusion. All procedures were conducted under the UT Health San Antonio approved Institutional Animal Care and Use Committee (IACUC) protocol 20210080AR.

After the heart was removed and placed in a surgical bowl, the aorta and the coronary sinus were cannulated using sterile zip ties. The heart was placed into the VP.S ENCORE® perfusion device filled with 3 L of Krebs-Henseleit buffer supplemented with 20PEG and hemoglobin-based oxygen carrier (HBOC). The heart was perfused with a pressure of approximately <20 mmHg resulting in a coronary perfusate flow of 50-100 mL/min for up to 8.5 hours at a 20-23°C temperature. At hour three post perfusion initiation, 3 mL of 3% lactic acid containing 135 mg of SNC80 (100 μM final concentration) was administered through arterial line followed by the 3 mL of Krebs-Henseleit flush. Post drug administration, the heart continued to be perfused for additional 5 hours.

After preservation, hearts were placed on a Langendorff system with a perfusate mixture of 1:1 porcine blood and Krebs-Henseleit buffer. Myocardial oxygen consumption (MVO_2 mLO_2 /min / 100g) was calculated during an initial 30 min of rewarming stage (before defibrillation) and after defibrillation using two oxygen probes (Pyro FireSting™, placed in

arterial and venous effluent). Oxygen consumption was captured using the following formula, ([O_2]a- [O_2]v)/100 * Q)/heart weight) * 100. [O_2]a and [O_2]v are defined as oxygen content of arterial and venous perfusate respectively. [O_2] was calculated as (1.34 * Hb* SO_2) + (K * pO_2); where 1.34 is mL O_2 / Hb (g), Hb is the concentration of hemoglobin measured in g/dL, SO_2 is the oxygen saturation ratio calculated using the equation developed by Severinghaus[48], K is the oxygen solubility coefficient adjusted for the perfusate temperature at every data point, pO_2 is the partial pressure of oxygen in mmHg for the perfusate sample, and Q is coronary flow in mL/min. The left ventricular function was expressed as dP/dT (mmHg/sec) measured by placing a pressure catheter (Millar, 5F) in the left ventricle. Data was analyzed using PowerLab (LabChart 8.1.16) blood pressure analyzer. Data was selected from the left ventricular pressure waveform as the average of 30 beats after stabilization (approx. 30 minutes after defibrillation). Contractility after ionotropic support was measured less than 5 minutes after administration of epinephrine (0.5mg injected arterial). End diastolic pressure of the left ventricle was maintained 5.14 +/- 1.89 mmHg through administering perfusate directly into the left ventricle through the pulmonary veins and venting to atmosphere.

Total RNA from cardiac tissue biopsies (2.5 mm) were extracted following the RNeasy Mini kit (Qiagen) according to the manufacturer's instructions. The concentration of total RNA was evaluated and measured at 260/280nm by spectrophotometer (NanoVue Plus, GE Healthcare). Synthesis of cDNA was performed from 0.5 µg of total RNA, which was reverse transcribed using (iScript cDNA Synthesis Kit, Bio-Rad) according to the manufacturer's instructions. Gene-specific pre-designed oligonucleotide primers were purchase from Sigma. qRT-PCR was done using SsoAdvanced Universal SYBR Green Supermix and SFX96 Touch real time PCR detection system (Bio-Rad, T100 Thermal Cycler). The cycling parameters were as follows: initial denaturation 95°C, 2 min; denaturation 95°C, 5 s; annealing/extension 60°C, 30 s; number of cycles 40; melt curve 65°-95°C (0.5°C increments). The comparative CT (2-

ΔΔCT) method was used for all quantification. Values were normalized to the Gapdh housekeeping gene.

Porcine limb ex vivo perfusion studies: Hindlimbs (N=8) were procured via protocol tissue sharing at the Joint Base San Antonio Clinical Investigation and Research Support (CIRS) building, following IV Pentobarbital euthanasia, 100 mg/kg from a host protocol. Host protocol animals were treated with the same surgical manipulations and no chemicals or drugs were introduced experimentally prior to euthanasia. Following euthanasia, a curvilinear incision was made around the hindlimb circumferentially. Subsequently, the neurovascular pedicle in the medial hindlimb was identified and carefully dissected out to preserve the vascular bundle. The pedicle was then divided at the origin of the artery and vein to preserve maximal length of the vessels. Hindlimb bone was separated using a Gigli Saw. Hindlimbs were cannulated through the femoral artery and underwent immediate arterial flush with up to 200-400 mL heparinized-saline solution (10,000 units of heparin per 1L of saline), until venous outflow was clear. Additionally, the femoral vein was cannulated for measurement and collection of venous outflow samples.

Limbs were divided into two groups, control (N=3) and experimental SNC80 (N=5). All hindlimbs were connected to the ENCORE™ head for perfusion via the cannulated femoral artery. The femoral vein was cannulated for obtaining venous samples. Hindlimbs were perfused with oxygenated Krebs-Henseleit (KH) at ambient temperature. Arterial and venous pO2 were assessed hourly using a commercial blood gas analyzer (ALB1000 by Radiometer, Brea, California USA). Oxygen consumption was calculated from A-V differences obtained from arterial and venous blood gas readings. After 3 hours of perfusion (baseline), torpor inducing compound SNC80 (44.96 μg/ml) was administered via the femoral artery to the experimental group (SNC80) (N=5) and an equal volume of the sham vehicle to the control limbs (N=3) followed by and additional 3 hours of perfusion (drug). The hind limbs were then removed from the perfusor and flushed with fresh KH perfusate and replaced into the perfusor containing fresh

KH solution (flush). The perfusion then resumed for an additional 6 hours. The hindlimbs were weighed pre and post perfusion. Biopsy tissue samples were taken at baseline (pre-ENCORE™), and before and after the administration of the SNC80 compound for RNA-Seq analysis and histological evaluation.

Biopsies for histopathology were obtained superficially from the rectus femoris muscle bundle immediately after amputation and then 24 hours after the perfusion period. Biopsies were stored in 10% formalin for 24 hours and then stored for 3 days in 70% ethanol and embedded in paraffin. The samples were sectioned into 5μm slides and stained with hematoxylin and eosin (H&E) to evaluate tissue morphology, intracellular distance, muscle bundle area, and Periodic Acid-Schiff to evaluate glycogen content. Histological analysis was performed by visualizing slides under a light microscope (AM Scope T670Q, Irvine, California) and capturing images using a high-definition camera (AM Scope Model# MU2003B1, Irvine, California). From each slide, 10 digital images from randomly selected fields were obtained at 10x magnification. The images were de-identified and evaluated for intracellular distance, muscle bundle area and glycogen content by two independent reviewers using Image J software (v.1.51.).

Statistical analysis. All graphing and statistical analyses were performed with Prism 9 (GraphPad Software Inc., La Jolla, CA, USA) with a (two-sided) significance level of 0.05. Statistical tests and corrections for multiple comparisons are described in each figure panel.

Data availability statement

The proteomics data reported in this paper have been deposited in the Mass Spec Interactive Virtual Environment, MassIVE, (accession no. XXX). All other data are available within the paper and its Supplementary Information files.

Software availability statement

No new software was generated.

Acknowledgements

The authors gratefully acknowledge funding from the Army Research Office/DARPA under Cooperative Agreement Number W911NF-19-2-0027. The views and conclusions contained in this document are those of the authors and should not be interpreted as representing the official policies, either expressed or implied, of the Army Research Office/DARPA or the U.S. Government. The U.S. Government is authorized to reproduce and distribute reprints for Government purposes notwithstanding any copyright notation herein. We thank E. Switzer for Xenopus embryo fertilization; R. Colon, S. Sundar, and E. Lederer for Xenopus embryo husbandry and transport organization; members of the Levin Lab, Tufts University for useful discussions; and R. Gould for help with database extraction. Image analysis workflows were created in consultation with D. Stirling and B. Cimini of the Broad Institute Imaging Platform. Biorender (https://biorender.com/) was used for the making of the schematic in Figure 4d.

Author Contributions

R.N., M.Su., and D.E.I. conceived of and directed the work. M.M.S., H.F., E.G., A.K., S.K., and T.L. performed *Xenopus* studies with guidance from R.N. and M.Lev. R.M. developed and maintained engineered components for *Xenopus* assays. H.F., M.M.S., A.K. and T.T. analyzed *Xenopus* data. T.L. and M.Lew. performed MALDI-TOF experiments and analyzed the data. B.C., K.P., and Z.I. performed in vitro and Organ Chip studies and analyzed data with guidance from A.M.S. S.M. and K.S. designed, assembled, and maintained custom microscopy equipment for Organ Chip imaging. K.S. analyzed imaging data from in vitro experiments. S.L. oversaw compound management and material transfers. Porcine heart experiments were conceived and directed by R.V. and L.B and experiments were designed and interpreted by

R.V., L.B., and K.A. Porcine heart data analysis was performed by R.V., L.B., K.A, E.C., R.L., I.C., and Z.M. Porcine heart data was acquired by K.A, E.C., R.L., I.C., and Z.M. Porcine limb studies were conceived and directed by R.V., L.B., E.W., and T.P. Porcine limb surgeries were performed by J.Y., O.P., and J.S. Porcine limb sampling and data analysis were performed by R.V., L.B., J.P., D.W., Z.H., C.H. and J.C.H. M.M.S., B.C., K.P., Z.I., T.L., K.A., R.N. and D.E.I. drafted the manuscript and all authors reviewed and provided critical input for the manuscript.

Competing Interests

D.E.I. is a founder, board member and Scientific Advisory Board chair of, and holds equity in, Emulate Inc. M.Le., R.N., M.M.S., E.G., T.T., and D.E.I are inventors on a relevant patent application held by Harvard University (PCT/US2021/012626). R.V., L.B., K.A, E.C., R.L., I.C., and Z.M are employees of Vascular Perfusion Solutions. The remaining authors declare no competing interests.

References

1. Vela, R. J., Jessen, M. E. & Peltz, M. Ice, ice, maybe? Is it time to ditch the igloo cooler? Benefits of machine perfusion preservation of donor hearts. *Artificial Organs* vol. 44 220–227 Preprint at https://doi.org/10.1111/aor.13599 (2020).
2. Petrenko, A. *et al.* Organ Preservation into the 2020s: The Era of Dynamic Intervention. *Transfusion Medicine and Hemotherapy* vol. 46 151–172 Preprint at https://doi.org/10.1159/000499610 (2019).
3. Guibert, E. E. *et al.* Organ preservation: Current concepts and new strategies for the next decade. *Transfusion Medicine and Hemotherapy* vol. 38 125–142 Preprint at https://doi.org/10.1159/000327033 (2011).
4. Andrijevic, D. *et al.* Cellular recovery after prolonged warm ischaemia of the whole body. *Nature* (2022) doi:10.1038/s41586-022-05016-1.
5. Tessier, S. N. *et al.* Partial freezing of rat livers extends preservation time by 5-fold. *Nat Commun* **13**, 4008 (2022).
6. Hrvatin, S. *et al.* Neurons that regulate mouse torpor. *Nature* **583**, 115–121 (2020).
7. Takahashi, T. M. *et al.* A discrete neuronal circuit induces a hibernation-like state in rodents. *Nature* **583**, 109–114 (2020).
8. Dou, M., Lu, C. & Rao, W. Bioinspired materials and technology for advanced cryopreservation. *Trends in Biotechnology* vol. 40 93–106 Preprint at https://doi.org/10.1016/j.tibtech.2021.06.004 (2022).
9. Blackstone, E., Morrison, M. & Roth, M. B. H2S induces a suspended animation-like state in mice. *Science (1979)* **308**, 518 (2005).
10. Beal, E. W. *et al.* [D-Ala 2 , D-Leu 5] Enkephalin Improves Liver Preservation During Normothermic Ex Vivo Perfusion. *Journal of Surgical Research* **241**, 323–335 (2019).
11. Ratigan, E. D. & McKay, D. B. Exploring principles of hibernation for organ preservation. *Transplantation Reviews* vol. 30 13–19 Preprint at https://doi.org/10.1016/j.trre.2015.08.002 (2016).
12. Rawls, S. M., Hewson, J. M., Inan, S. & Cowan, A. Brain delta2 opioid receptors mediate SNC-80-evoked hypothermia in rats. *Brain Res* **1049**, 61–69 (2005).
13. Horiuchi, T. *et al.* The Effects of the δ-Opioid Agonist SNC80 on Hind-Limb Motor Function and Neuronal Injury After Spinal Cord Ischemia in Rats. *Anesth Analg* **99**, 235–240 (2004).
14. Sperry, M. M. *et al.* Enhancers of host immune tolerance to bacterial infection discovered using linked computational and experimental approaches. *Advanced Science* (2022).
15. Novak, R. *et al.* Target-agnostic discovery of Rett Syndrome therapeutics by coupling computational network analysis and CRISPR-enabled in vivo disease modeling. *bioRxiv* (2022) doi:10.1101/2022.03.20.485056.
16. Schmitt, S. M., Gull, M. & Brändli, A. W. Engineering Xenopus embryos for phenotypic drug discovery screening. *Adv Drug Deliv Rev* **69–70**, 225–246 (2014).
17. Sullivan, K. G. & Levin, M. Inverse drug screening of bioelectric signaling and neurotransmitter roles: Illustrated using a Xenopus tail regeneration assay. *Cold Spring Harb Protoc* **2018**, 154–163 (2018).
18. Giroud, S. *et al.* Lipidomics reveals seasonal shifts in a large-bodied hibernator, the brown bear. *Front Physiol* **10**, (2019).
19. Kolomiytseva, I. K. Lipids in mammalian hibernation and artificial hypobiosis. *Biochemistry (Moscow)* vol. 76 1291–1299 Preprint at https://doi.org/10.1134/S0006297911120029 (2011).
20. Soeters, M. R. *et al.* Muscle acylcarnitines during short-term fasting in lean healthy men. *Clin Sci* **116**, 585–592 (2009).

21. Welinder, K. G. *et al.* Biochemical foundations of health and energy conservation in hibernating free-ranging subadult brown bear ursus arctos. *Journal of Biological Chemistry* **291**, 22509–22523 (2016).
22. Otis, J. P., Sahoo, D., Drover, V. A., Yen, C. L. E. & Carey, H. v. Cholesterol and lipoprotein dynamics in a hibernating mammal. *PLoS One* **6**, (2011).
23. Jones, L. L., McDonald, D. A. & Borum, P. R. Acylcarnitines: Role in brain. *Progress in Lipid Research* vol. 49 61–75 Preprint at https://doi.org/10.1016/j.plipres.2009.08.004 (2010).
24. Petrov, A., Kasimov, M. & Zefirov, A. Brain Cholesterol Metabolism and Its Defects: Linkage to Neurodegenerative Diseases and Synaptic Dysfunctio. *Acta Naturae* **8**, 58–73 (2016).
25. Ingber, D. E. Human organs-on-chips for disease modelling, drug development and personalized medicine. *Nature Reviews Genetics* vol. 23 467–491 Preprint at https://doi.org/10.1038/s41576-022-00466-9 (2022).
26. Klepinina, L. *et al.* Colon cancer cell differentiation by sodium butyrate modulates metabolic plasticity of Caco-2 cells via alteration of phosphotransfer network. *PLoS One* **16**, e0245348 (2021).
27. Mookerjee, S. A. & Brand, M. D. Measurement and analysis of extracellular acid production to determine glycolytic rate. *J. Vis. Exp.* **2015**, 1–9 (2015).
28. Costa, C., Huneau, J. F. & Tomé, D. Characteristics of L-glutamine transport during Caco-2 cell differentiation. *Biochim. Biophys. Acta - Biomembr.* **1509**, 95–102 (2000).
29. Souba, W. W. *et al.* The role of glutamine in maintaining a healthy gut and supporting the metabolic response to injury and infection. *J. Surg. Res.* **48**, 383–391 (1990).
30. Si, L. *et al.* A human-airway-on-a-chip for the rapid identification of candidate antiviral therapeutics and prophylactics. *Nat Biomed Eng* (2021) doi:10.1038/s41551-021-00718-9.
31. Kim, H. J., Li, H., Collins, J. J. & Ingber, D. E. Contributions of microbiome and mechanical deformation to intestinal bacterial overgrowth and inflammation in a human gut-on-a-chip. *Proc Natl Acad Sci U S A* **113**, E7–E15 (2016).
32. Choi, Y. Y., Kim, J., Lee, S. H. & Kim, D. S. Lab on a chip-based hepatic sinusoidal system simulator for optimal primary hepatocyte culture. *Biomed Microdevices* **18**, (2016).
33. Ewart, L. *et al.* Qualifying a human Liver-Chip for predictive toxicology: Performance assessment and economic implications. *bioRxiv* 2021.12.14.472674 (2021) doi:10.1101/2021.12.14.472674.
34. Yang, Y. *et al.* Mitochondrial UQCC3 Modulates Hypoxia Adaptation by Orchestrating OXPHOS and Glycolysis in Hepatocellular Carcinoma. *Cell Rep* **33**, 108340 (2020).
35. Kaltenborn, A. *et al.* Ex vivo limb perfusion for traumatic amputation in military medicine. *Mil Med Res* **7**, (2020).
36. Magi, S. *et al.* Glutamate-induced ATP synthesis: Relationship between plasma membrane Na+/Ca2+ exchanger and excitatory amino acid transporters in brain and heart cell models. *Mol Pharmacol* **84**, 603–614 (2013).
37. Magi, S., Piccirillo, S. & Amoroso, S. The dual face of glutamate: from a neurotoxin to a potential survival factor—metabolic implications in health and disease. *Cellular and Molecular Life Sciences* vol. 76 1473–1488 Preprint at https://doi.org/10.1007/s00018-018-3002-x (2019).
38. Magi, S., Piccirillo, S. & Amoroso, S. The dual face of glutamate: from a neurotoxin to a potential survival factor—metabolic implications in health and disease. *Cell. Mol. Life Sci.* **76**, 1473–1488 (2019).

39. Kon, N. *et al. Na + /Ca 2+ exchanger mediates cold Ca 2+ signaling conserved for temperature-compensated circadian rhythms*. *Sci. Adv* vol. 7 http://advances.sciencemag.org/ (2021).
40. Shah Amran, M., Homma, N. & Hashimoto, K. *Pharmacology of KB-R7943: A Na +-Ca 2+ exchange inhibitor-sion arrhythmia-KB-R7943-Na +-Ca 2+ exchange (NCX1-3)-NCX inhibitors-Ni 2+-SEA0400-SN-6*. (2003).
41. Schafer, C. *et al. Role of the reverse mode of the Na / Ca exchanger in reoxygenation-induced cardiomyocyte injury*. *Cardiovascular Research* vol. 51 www.elsevier.com/locate/cardiores (2001).
42. Wan, H. *et al.* NCX1 coupled with TRPC1 to promote gastric cancer via Ca2+/AKT/β-catenin pathway. *Oncogene* (2022) doi:10.1038/s41388-022-02412-9.
43. Bankhead, P. *et al.* QuPath: Open source software for digital pathology image analysis. *Sci Rep* **7**, (2017).
44. Goto-Inoue, N., Kashiwagi, A., Kashiwagi, K. & Mori, T. Metabolomic approach for identifying and visualizing molecular tissue markers in tadpoles of Xenopus tropicalis by mass spectrometry imaging. *Biol Open* **5**, 1252–1259 (2016).
45. Berg, J., Hung, Y. P. & Yellen, G. A genetically encoded fluorescent reporter of ATP:ADP ratio. *Nat. Methods* **6**, 161–166 (2009).
46. Stirling, D. R. *et al.* CellProfiler 4: improvements in speed, utility and usability. *BMC Bioinformatics* **22**, (2021).
47. Henry, O. Y. F. *et al.* Organs-on-chips with integrated electrodes for trans-epithelial electrical resistance (TEER) measurements of human epithelial barrier function. *Lab Chip* **17**, 2264–2271 (2017).
48. Severinghaus, J. W. *Simple, accurate equations for human blood 02 dissociation computations*. (1979).

Figure Legends

Figure 1. SNC80 treatment in *Xenopus* tadpoles. a. Swimming activity of *Xenopus* during 100μM SNC80 or vehicle treatment. Data represent the mean±SD of n=3 replicates, with 10 tadpoles per replicate. **b.** Oxygen consumption rate for *Xenopus* treated with SNC80 or vehicle controls. N=4 vehicle and n=7 SNC80, with each data point representing the cumulative oxygen consumption for 5 tadpoles. **c.** Heart rate in SNC80 and vehicle-treated *Xenopus* (n=10 tadpoles/group). **d.** Distribution of SNC80 in *Xenopus* tadpoles after 1 and 2 hours of compound exposure. **e.** Oxygen consumption in *Xenopus* tadpoles treated with SNC80, the delta opioid antagonist naltrindole, or a combination of SNC80 and naltrindole. N=3 replicates/group with each data point representing the cumulative oxygen consumption from 5 tadpoles. Statistical comparisons were performed using an unpaired t-test (b,c) and a Brown-Forsythe and Welch ANOVA test with Dunnett correction for multiple comparisons between vehicle and each treatment group (e). Bar plots show the mean±SD of each group.

Figure 2. SNC80 treatment in cell culture and Organ Chip systems. a. Oxygen consumption rate (OCR) and mitochondrial ATP production obtained with Seahorse measurements for Caco-2 intestinal epithelium (filled circle), HUVEC (empty circles), Huh7 liver epithelium (filled squares) and LSEC (empty squares) after 2h 100μM SNC80 treatment (n=3-4 biological replicates/cell type). Values are normalized to their respective vehicle controls. **b.** Graph showing the quantitative drop in ATP/ADP ratio of Huh7 cells treated with 100μM SNC80 (n=2 control and n=3 SNC80 biological replicates). **c.** Monitoring changes in O_2 level on sensor Gut (dotted lines; n=6 Chips/group) or Liver (straight lines; n=15-16 Chips/group) Chip throughout the treatment with 100μM SNC80 (0-48h) and recovery (48-120h) versus vehicle control Chip. **d.** Graph showing the quantitative drop in ATP/ADP ratio of Liver Chip treated for 48h with 100μM SNC80 or Vehicle control as well as 2 days recovery after drug washout (n=5 control and n=3 SNC80 Chips). Statistical comparisons were performed using a two-way

ANOVA with Dunnett correction with multiple comparison control vs treatment for each dataset (a,b) and multiple unpaired t-tests for each timestamp with multiple comparison between control and treated cells (c,d). Data represent the mean±SD.

Figure 3. Preservation of porcine cardiac grafts with SNC80. a. Relative metabolic rate at baseline (3 hours) and during treatment (5 hours) for vehicle and SNC80-treated cardiac grafts perfused in the VP.S ENCORE® device (n=2 hearts/group over 13 measurement time points). **b.** Oxygen consumption during cardiac reperfusion on the Langendorff system before defibrillation (n=2 vehicle and n=3 SNC80 hearts). **c.** Oxygen consumption measured on the Langendorff system after defibrillation (n=2 vehicle and n=3 SNC80 hearts). **d.** Left ventricle (LV) contractility before and after defibrillation and tissue exposure to epinephrine (n=2 vehicle and n=3 SNC-treated hearts). **e.** Gene expression analysis of heart biopsy samples for vehicle and SNC80-treated cardiac grafts (n=4 biological replicates/group). Statistical comparisons were performed using a two-way ANOVA with Sidak correction for multiple comparisons between SNC80 and vehicle-treated cardiac grafts (a,d), a mixed effects analysis with Sidak correction for multiple comparisons between SNC80 and vehicle-treated cardiac grafts (b,c), and unpaired t-tests between SNC80 and vehicle for each gene of interest (e). Data represent the mean±SD.

Figure 4. SNC80 biostasis induction mechanisms. a. Thermal proteome profiling (TPP) melting point differences between vehicle controls and SNC80-treated *Xenopus* for the membrane transport proteins EAAT1 and NCX1 (n=3 tadpoles/group/temperature). **b.** *Xenopus* movement during treatment with DL-TBOA (n=80 tadpoles) and aprindine (n=40 tadpoles), which block EAATs and NCX, respectively. **c.** Oxygen consumption rates for *Xenopus* exposed to DL-TBOA (n=4-5 replicates/group) and aprindine (n=3 replicates/group). Each data point represents the cumulative oxygen consumption for 5 tadpoles. **d.** Proposed mechanism of action for SNC80 at the mitochondrial membrane. Collectively, data suggests that SNC80

interferes in calcium transport by NCX, thereby suppressing downstream ATP production by the electron transport chain (ETC). Statistical comparisons were performed using a t-test and FDR correction over all proteins assessed (a), separate one-way ANOVAs with Dunnett correction for multiple comparisons between baseline and treatment/recovery for each compound (b), and separate unpaired t-tests comparing vehicle and treatment groups (c).

Supplemental Figure Legends

Figure S1. Metabolic measurements in SNC80-treated *Xenopus* embryos and tadpoles. a. Oxygen consumption rate in *Xenopus* embryos treated with SNC80 (n=3-4 replicates/group). Each data point represents the cumulative oxygen consumption for 5 tadpoles. **b.** *In vivo* distribution of SNC80 at 1 and 2 hours of exposure in *Xenopus* tadpoles. **c.** Uptake of SNC80 in the tadpole skeletal muscle, GI tract, and gills at 1 and 2 hours of exposure. **d.** Levels of acylcarnitine and cholesterol ester in the skeletal muscle and brain after 1 hour of SNC80 treatment. *In vivo* distributions of SNC80 and lipid levels measured from N=5 tadpoles per condition; N=3 sections/slide. Statistical comparisons were performed using a Brown-Forsythe and Welch ANOVA test with Dunnett correction for multiple comparisons between untreated and each treatment group (a), a two-way ANOVA (time x tissue region) with Sidak correction for multiple comparisons (c) and multiple unpaired t-tests for each tissue region with FDR correction (d). Data represent the mean±SD.

Figure S2. Metabolic measurements in gut and liver cultures treated with SNC80. a. Normalized cytotoxicity % for Caco2 intestinal epithelial cells (filled circles) or HUVECs (empty circles) as well as Huh7 liver epithelium (filled squares) or LSECs (empty squares) after 2 hours of exposure to 100μM SNC80 (n=3 biological replicates/cell type). **b.** Normalized ECAR, glutamate, and creatine kinase (CK) activity in for Caco2 intestinal epithelial cells (filled circles) and HUVECs (empty circles) as well as Huh7 liver epithelium (filled squares) and LSECs (empty squares) (n=3-6 biological replicates/measurement/cell type). **c.** Representative images of

ATP/ADP fluorescence intensity at T=0 and T=2 hours of vehicle (top) or SNC80 (bottom) treatment. Tones towards the red show more intensity, higher ATP/ADP ratio and higher metabolism. Statistical comparisons were performed using a two-way ANOVA with Dunnett correction with multiple comparison control vs treatment for each dataset (a,b). Data represent the mean±SD.

Figure S3. Characterization of Gut and Liver Chips with integrated sensing technology. a. Illustration of the sensor-integrated OOC unit connected to reservoir pod for automatic operation of fluid flow using pneumatic pressure (left). Inset shows a schematic of the top and bottom views of the sensor-chip-PCB compartment showing locations of TEER electrodes and O_2 sensors in the apical and basal channels. Four O_2 sensing spots were added to the channels - two in the top and two in the bottom channels for across the chip measurement. Electrode connectors are necessary for remote TEER sensing. **b.** Phase contrast images of Caco-2 cells seeded on sensor-chip at day 1, and 10 of culture (top) and Huh7 cells seeded on sensor-chip at day 1 and 10 (middle). Fluorescent images of liver chip at day 1 and 10 of the transduced nuclear marker (bottom) **c.** Percentage of O2 level (black) and TEER impedance values (gray) on sensor Liver Chip during 10 days of culture. **d**. Average albumin production of Liver Chips at day of experiment start (day 7-10 of culture). **e**. Average urea production of Liver Chips at day of experiment start (day 7-10 of culture). **f.** Representative immunofluorescence images of the sensor Gut Chip (left) and Liver Chip (right) epithelium stained with DNA damage marker (H2AX) and nuclei (DAPI) for vehicle control and SNC80 treated tissues after 7 days recovery. **g.** Quantitative analysis of proliferation and DNA damage stains on Gut and Liver Chips after 48h of treatment and 7-day recovery to 100μM SNC80 (2-3 biological replicates/group/marker). Statistical comparisons were performed using multiple unpaired t-tests for each marker with FDR correction. Data represent the mean±SD.

Figure S4. Metabolic measurements of Gut and Liver Chip systems treated with SNC80. a. Monitoring the percentage change in barrier function of Gut (n=6 Chips/group) or **b**. Liver Chip (n=9 Chips/group) with time during treatment with 100μM SNC80 (0-48h) and recovery (48-120h) versus vehicle control Chip. **c**. Cytotoxicity measured for the Gut and **d.** Liver Chips during treatment and recovery. **e**. Graph depicting the amount of lactate measured in effluents of Gut and **f**. Liver Chips post recovery (day 7 for Gut and day 5 for Liver) for SNC80-treated (red) or vehicle control (black) Chips. **g**. Graph showing the glutamate measured in effluents of Gut or **h**. Liver Chips during SNC80 (red) or vehicle (black) treatment and post recovery (day 7). For each measurement, statistical comparisons were performed using multiple unpaired t-tests at each timepoint and FDR correction for multiple comparisons. Data represent the mean±SD.

Figure S5. Preservation of whole porcine limbs with SNC80. a. The relative metabolic rate at baseline is not statistically significantly different between control (n=3) and SNC80 (n=5) injected limbs. Metabolic rate is reduced during the treatment and washout phases for SNC80 relative to controls. **b.** Mean muscle bundle area between T0 before SNC80 administration and at T3 after SNC80 administration and histographs of limb biopsy (20x magnification) at T0 before SNC80 administration and T3 after SNC80 administration. Muscle bundle area is not affected by the administration of SNC80. **c.** Optical density between T0 before SNC80 administration and at T3 after SNC80 administration and histographs of limb biopsy (20x magnification) at T0 before SNC80 administration and T3 after SNC80 administration. Optical density is not affected by the administration of SNC80. **d.** Mean intracellular distance during T0 before SNC80 administration versus T3 after SNC80 administration and histographs of limb biopsy (10x magnification) at T0 before SNC80 administration and T3 after SNC80 administration. Red arrows indicate intracellular distance measured. Intracellular distance increases after the administration of SNC80. Statistical

comparisons were performed using a mixed-effects analysis with a Sidak test for multiple comparisons (a) and Welch's t-test (b-d). Data represent the mean±SD.

Figure S6. NCX blockade in *Xenopus* tadpoles. Tadpole movement at baseline, during treatment, and during recovery from **a.** KB-R7943 and **b.** dronedarone (n=40 tadpoles/treatment). Statistical comparisons were performed using separate one-way ANOVAs with Dunnett correction for multiple comparisons between baseline and treatment/recovery for each compound. Data represent the mean±SD.

Figure S7. NCX blockade in liver and gut cultures. a. Graph depicting oxygen consumption rate (OCR) and mitochondrial ATP production obtained with Seahorse measurements for Caco-2 intestinal epithelial cells (filled circle) and HUVECs (empty circles) after 2h of treatment with Aprindine 50μM (blue), KBR-9743 25μM (green) or dronedarone 25μM (pink). Values are normalized to their respective vehicle controls. **b**. Graph depicting oxygen consumption rate (OCR) and mitochondrial ATP production obtained with Seahorse measurements for Huh7 liver epithelium (filled circle) and LSECs (empty circles) after 2h of treatment with Aprindine 50μM (blue), KBR-9743 50μM (green filled circles), KBR-9743 100μM (green empty circles), dronedarone 50μM (green filled circles) or dronedarone 100μM (green empty circles). Values are normalized to their respective vehicle controls. Datapoints with red crosses describe that the cells did not recover after drug exposure, suggesting toxicity induced by KBR-9743 and dronedarone. N=3 biological replicates/cell type/treatment. Statistics used was two-way ANOVA with Dunnett correction with multiple comparison control vs treatment for each dataset. Data represent the mean±SD.

Table S1. SNC80 protein binding targets identified by thermal proteome profiling.

Table S2. Compound doses and sources for *Xenopus* and human cell culture experiments.

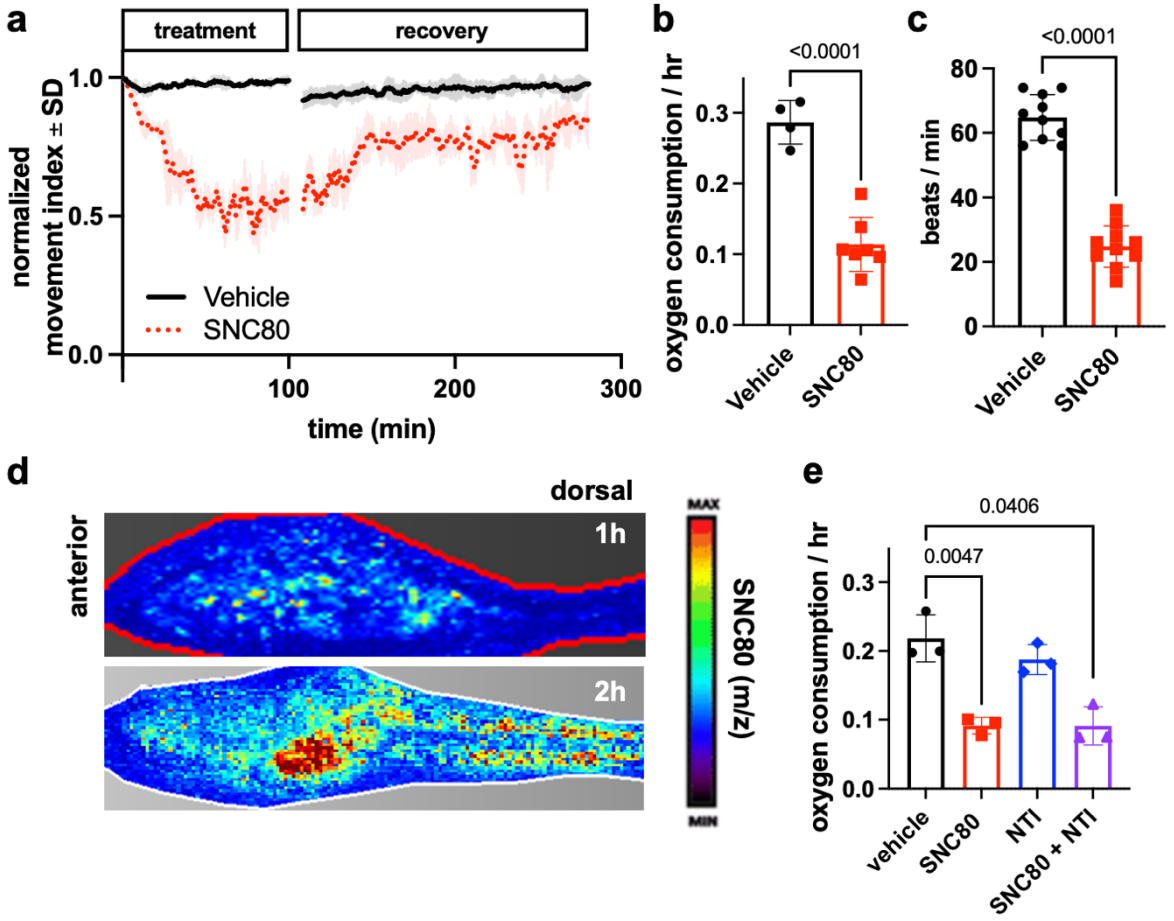
a
treatment
recovery
normalized movement index ± SD
1.0
0.5
0.0
Vehicle
SNC80
100
200
300
time (min)
b
<0.0001
oxygen consumption / hr
0.3
0.2
0.1
0.0
Vehicle
SNC80
c
<0.0001
beats / min
80
60
40
20
0
Vehicle
SNC80
d
dorsal
anterior
1h
2h
MAX
MIN
SNC80 (m/z)
e
0.0406
0.0047
oxygen consumption / hr
0.3
0.2
0.1
0.0
vehicle
SNC80
NTI
SNC80 + NTI

Figure 1

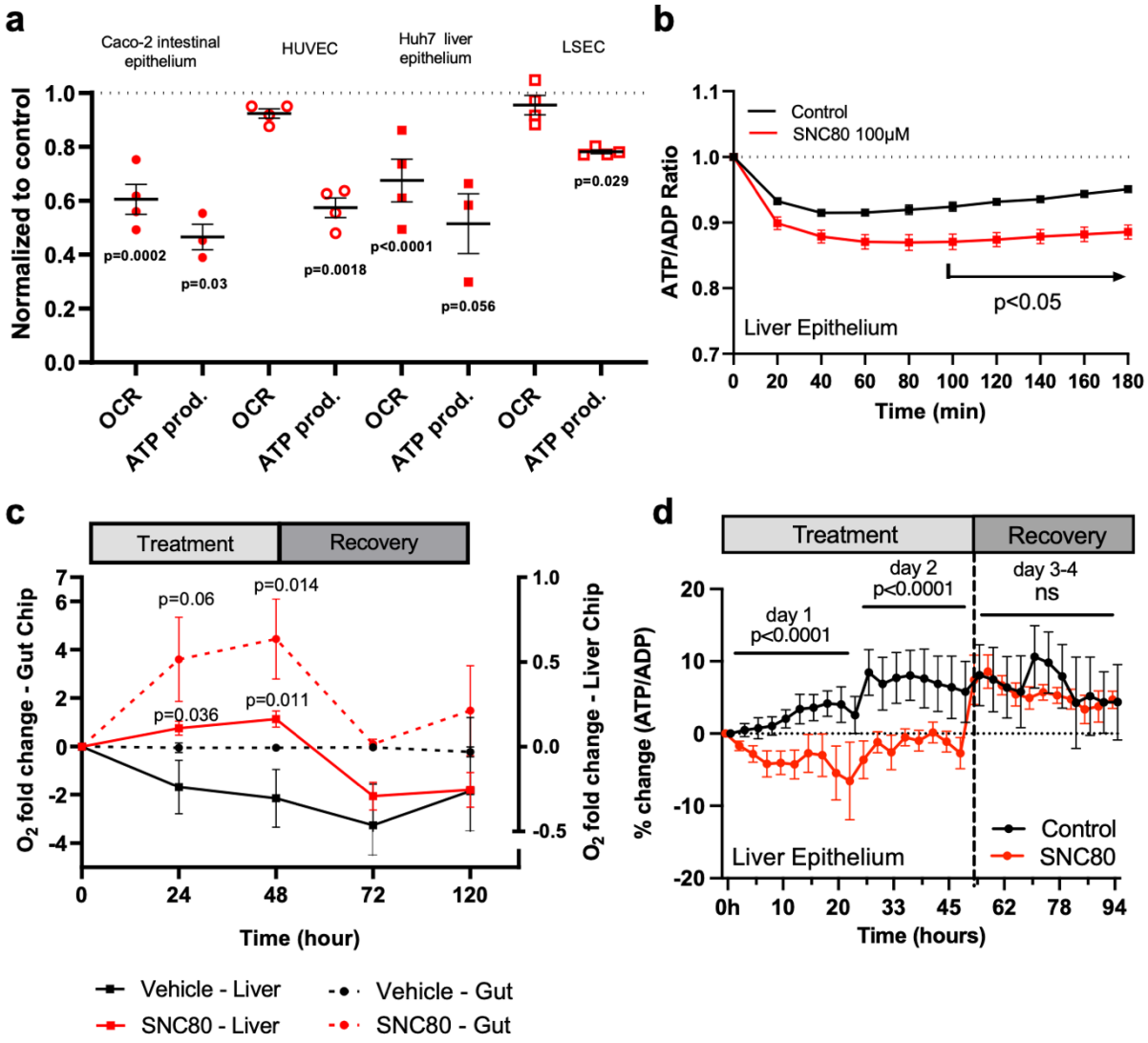
a
Caco-2 intestinal epithelium
HUVEC
Huh7 liver epithelium
LSEC
Normalized to control
p=0.0002
p=0.03
p=0.0018
p<0.0001
p=0.056
p=0.029
OCR
ATP prod.
b
Control
SNC80 100μM
ATP/ADP Ratio
p<0.05
Liver Epithelium
Time (min)
c
Treatment
Recovery
p=0.06
p=0.014
p=0.036
p=0.011
O2 fold change - Gut Chip
O2 fold change - Liver Chip
Time (hour)
Vehicle - Liver
SNC80 - Liver
Vehicle - Gut
SNC80 - Gut
d
Treatment
Recovery
day 1
p<0.0001
day 2
p<0.0001
day 3-4
ns
% change (ATP/ADP)
Liver Epithelium
Control
SNC80
Time (hours)

Figure 2

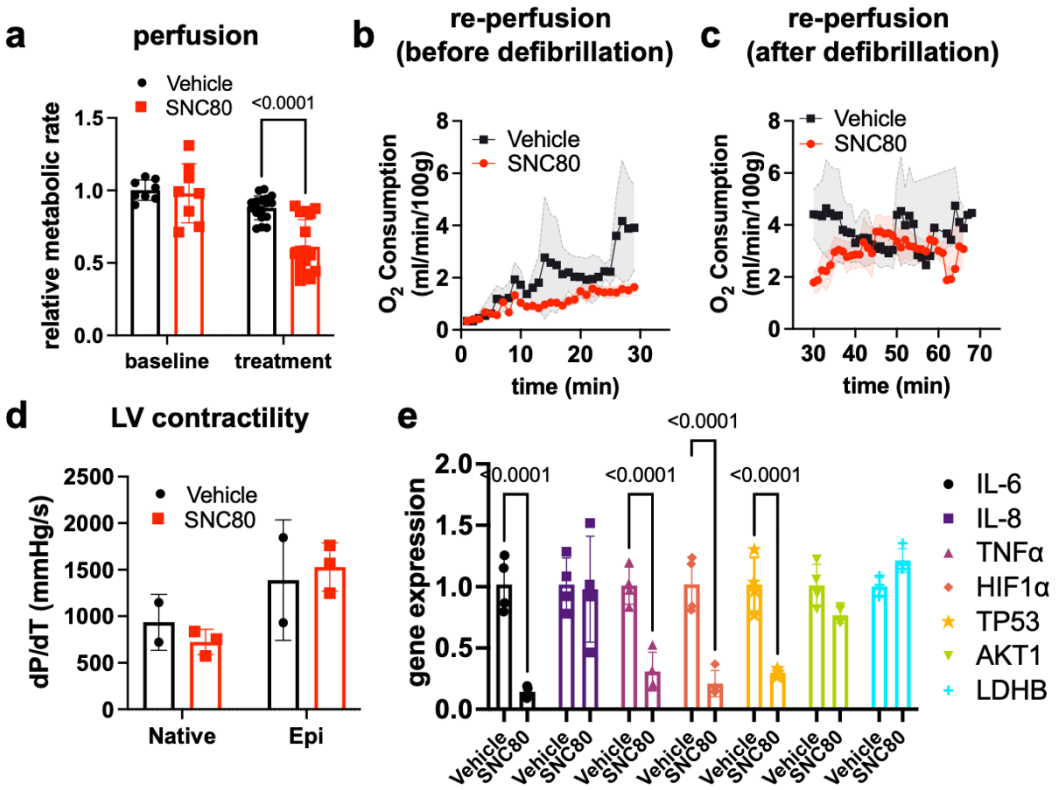
a
perfusion
Vehicle
SNC80
<0.0001
relative metabolic rate
1.5
1.0
0.5
0.0
baseline
treatment
b
re-perfusion
(before defibrillation)
Vehicle
SNC80
O2 Consumption
(ml/min/100g)
8
6
4
2
0
0
10
20
30
time (min)
c
re-perfusion
(after defibrillation)
Vehicle
SNC80
O2 Consumption
(ml/min/100g)
8
6
4
2
0
30
40
50
60
70
time (min)
d
LV contractility
Vehicle
SNC80
dP/dT (mmHg/s)
2500
2000
1500
1000
500
0
Native
Epi
e
<0.0001
<0.0001
<0.0001
<0.0001
gene expression
2.0
1.5
1.0
0.5
0.0
Vehicle
SNC80
IL-6
IL-8
TNFα
HIF1α
TP53
AKT1
LDHB

Figure 3

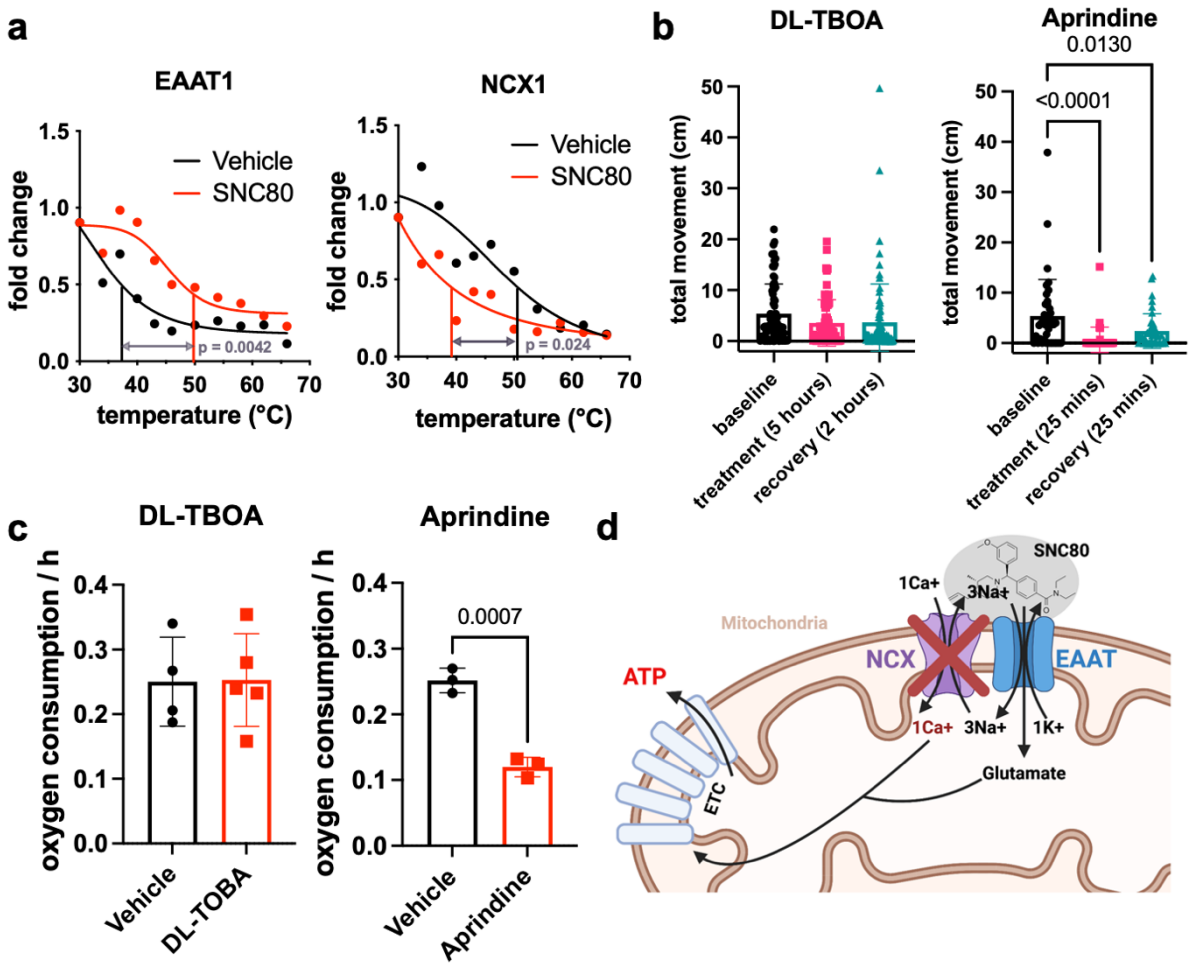
a
EAAT1
NCX1
Vehicle
SNC80
fold change
temperature (°C)
p = 0.0042
p = 0.024
b
DL-TBOA
Aprindine
0.0130
<0.0001
total movement (cm)
baseline
treatment (5 hours)
recovery (2 hours)
treatment (25 mins)
recovery (25 mins)
c
DL-TBOA
Aprindine
oxygen consumption / h
0.0007
Vehicle
DL-TOBA
Aprindine
d
SNC80
1Ca+
3Na+
Mitochondria
NCX
EAAT
ATP
1Ca+
3Na+
1K+
Glutamate
ETC

Figure 4

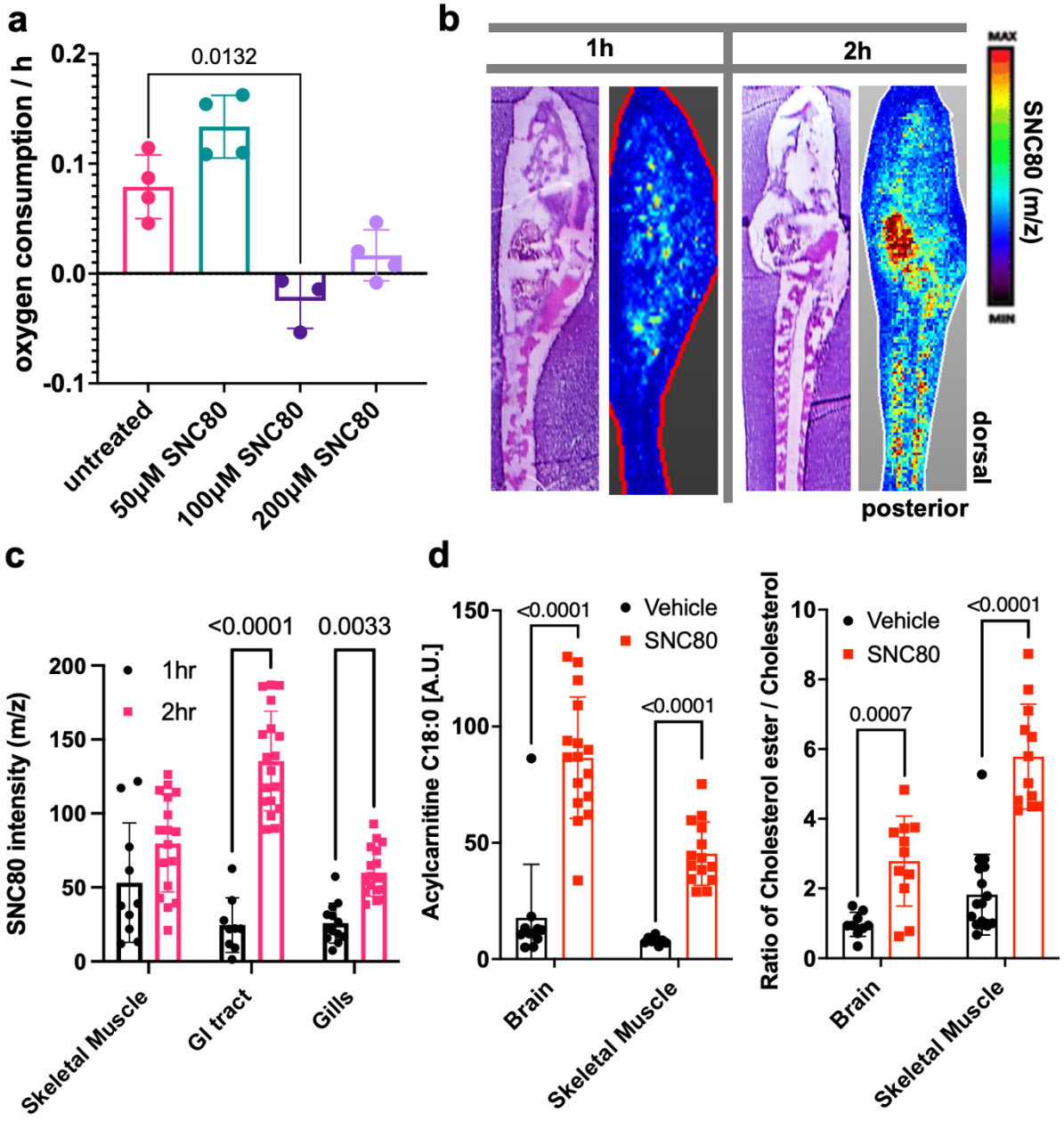

Supp. Figure S1

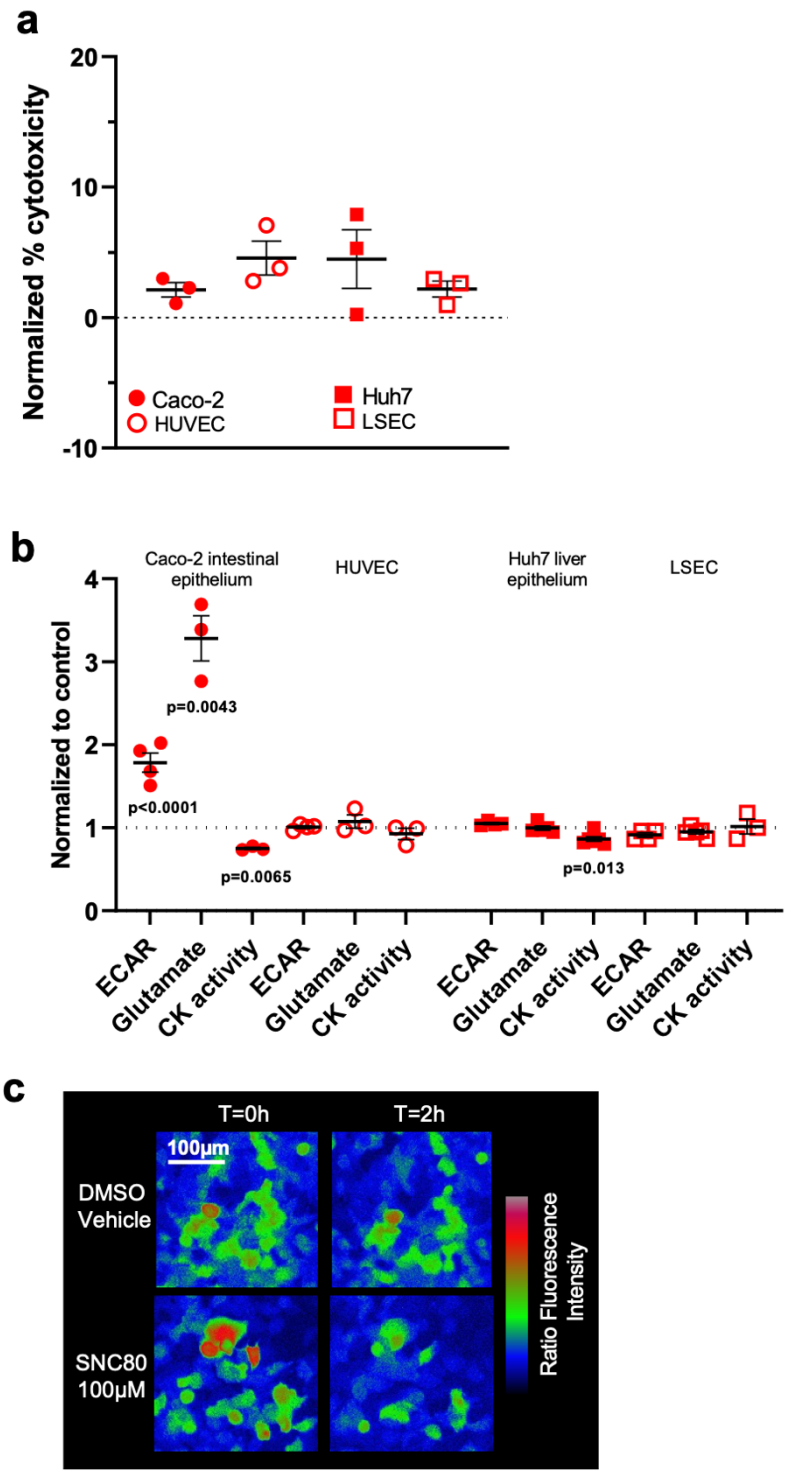

Supp. Figure S2

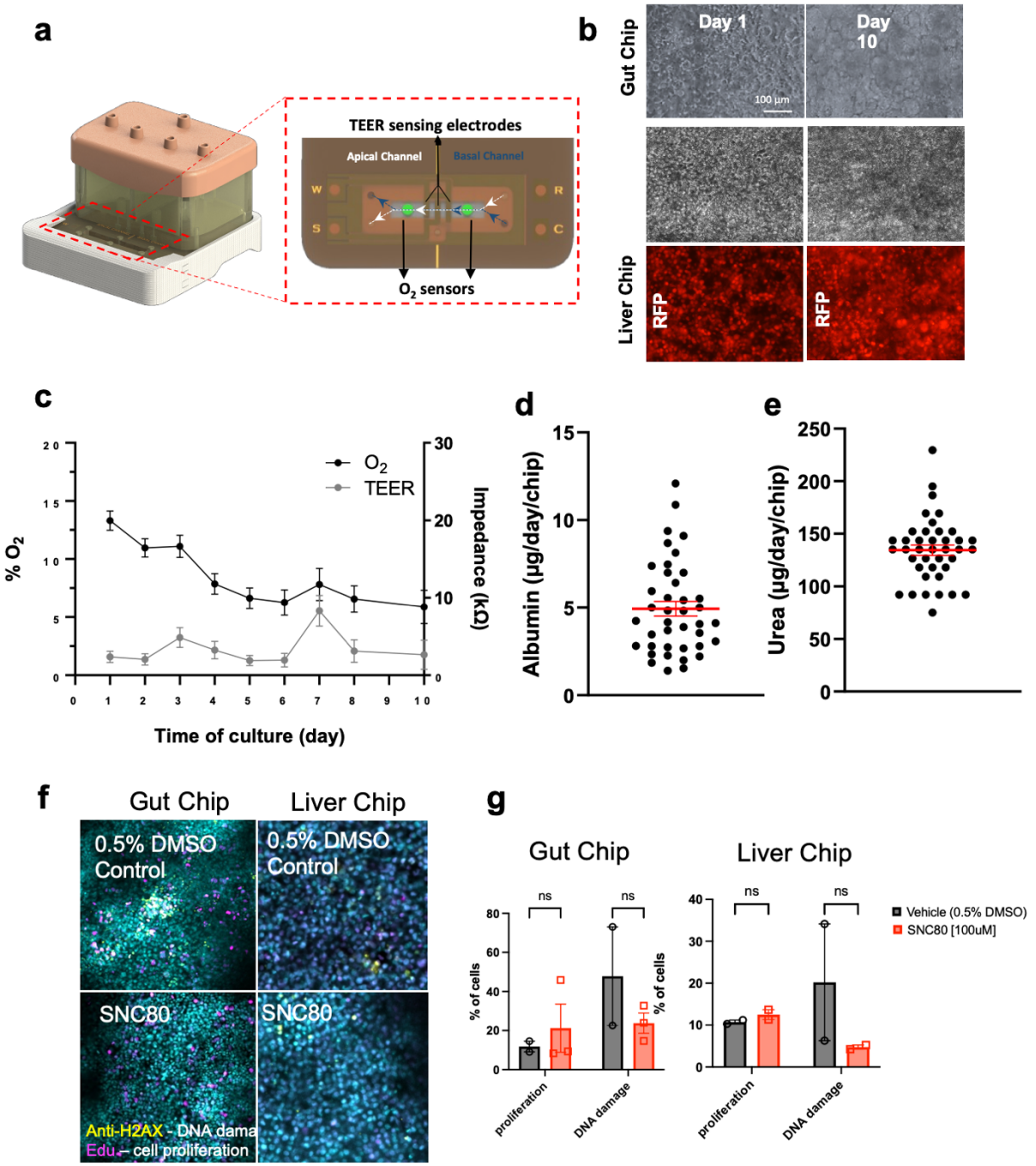

Supp. Figure S3

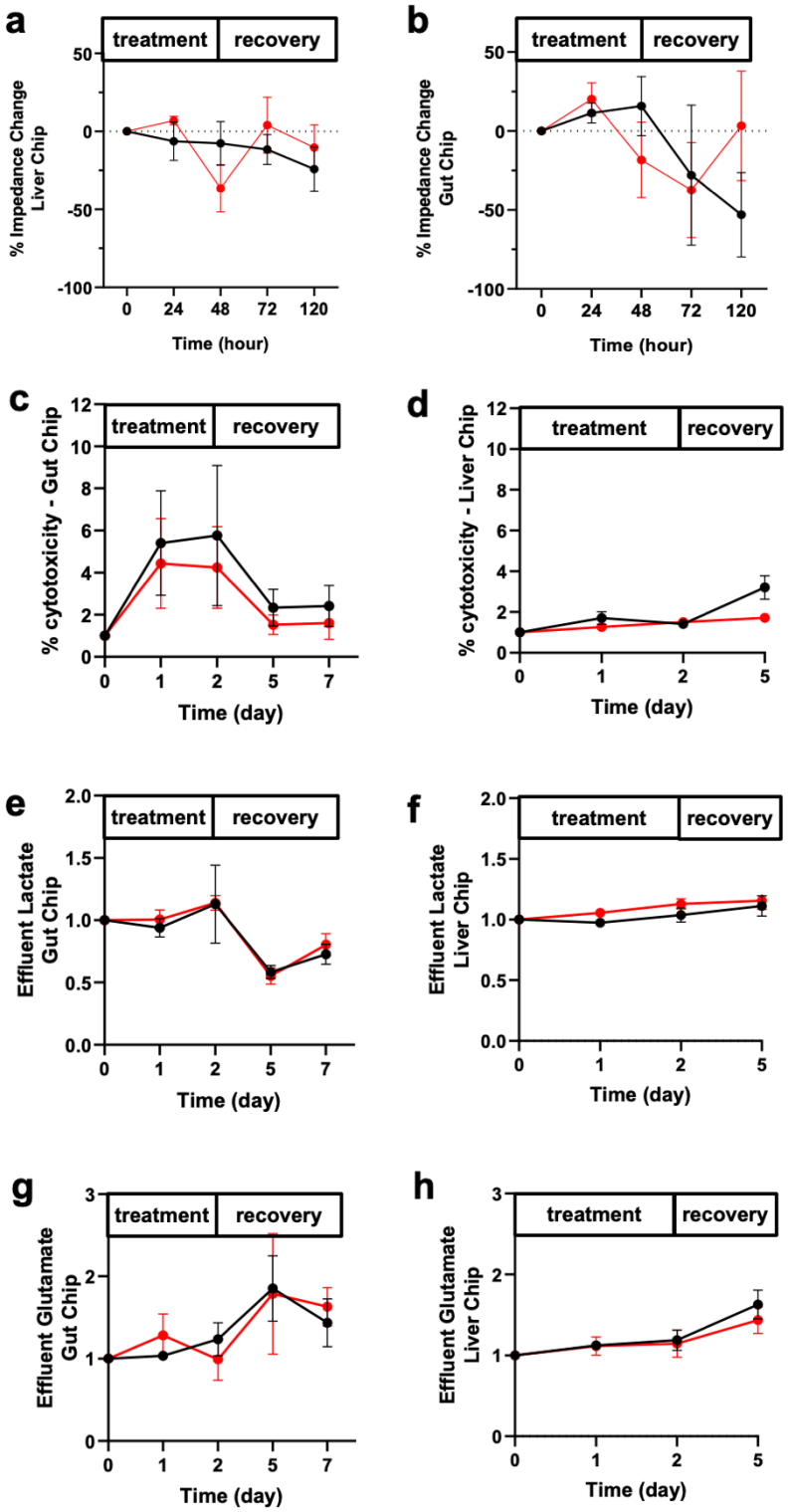

Supp. Figure S4

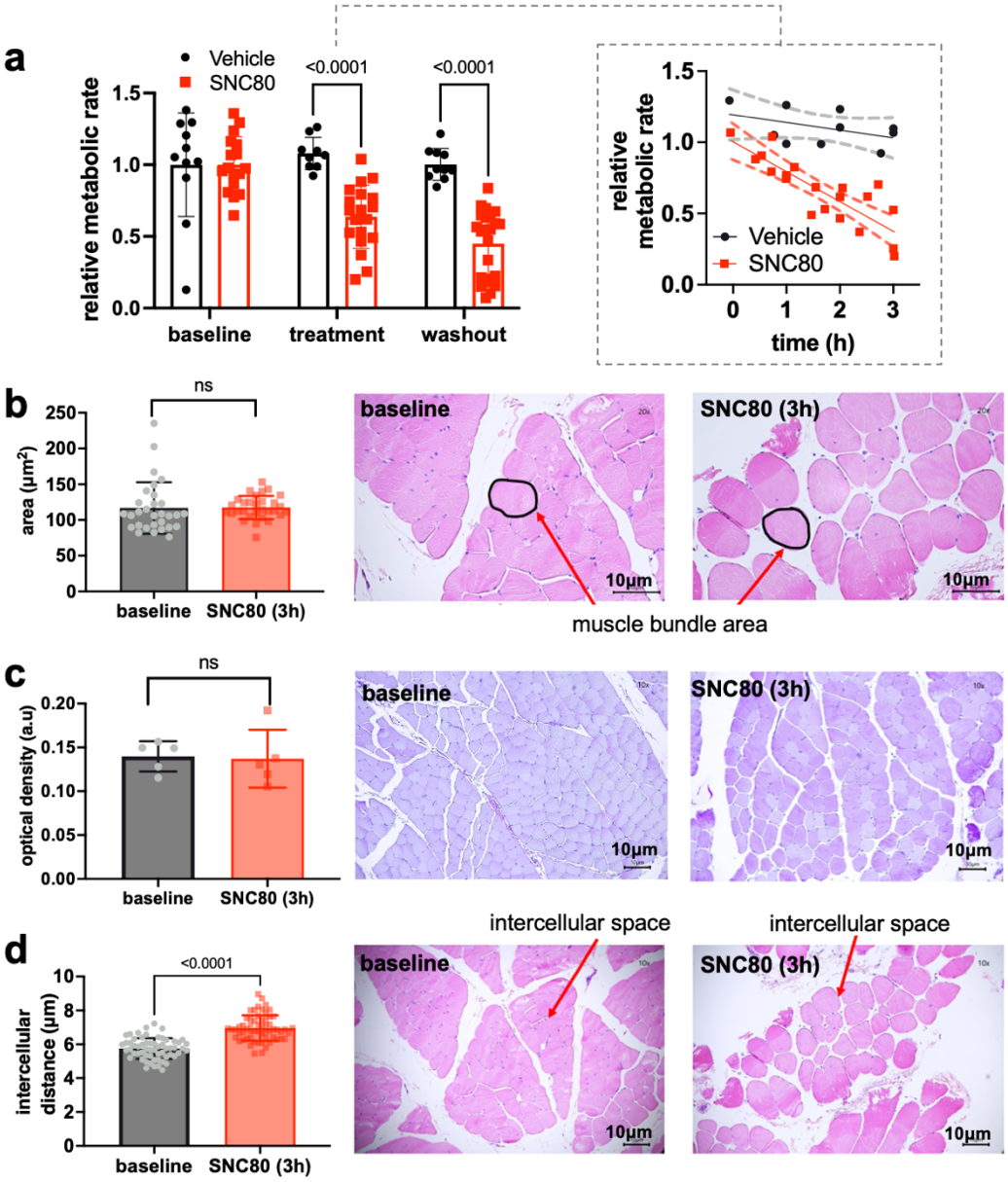

Supp. Figure S5

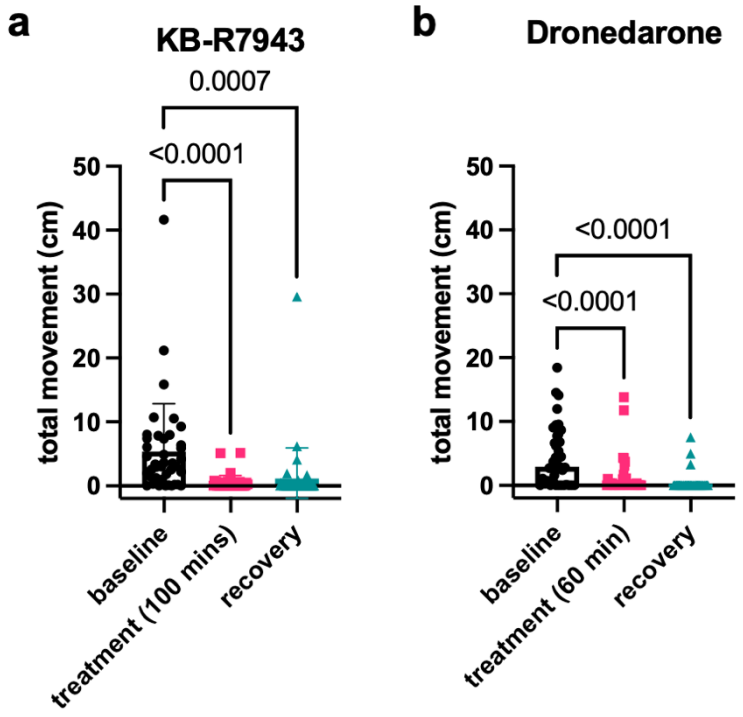

Supp. Figure S6

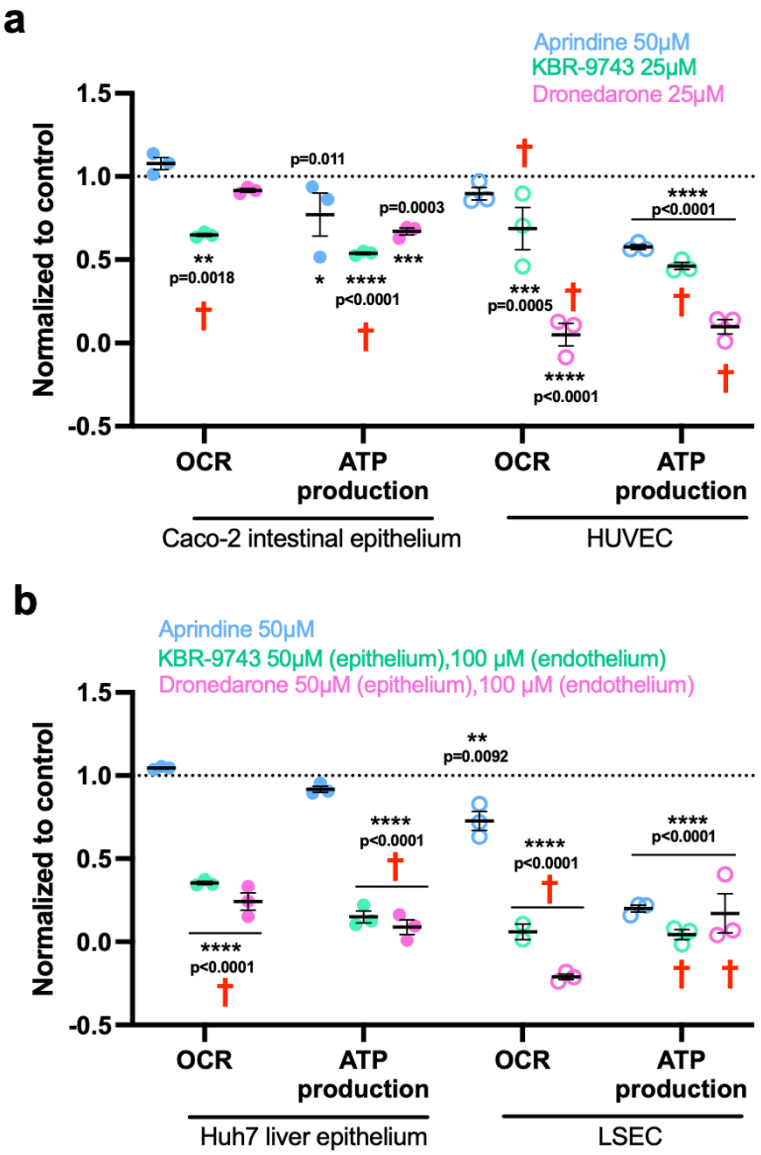

Supp. Figure S7

direct interaction	function	indirect interaction	function
CCBL1	• pyridoxal phosphate binding • cysteine-S-conjugate beta-lyase activity • L-glutamine aminotransferase activity • cellular modified amino acid metabolic process	ABCB1	• ABC-type bile acid transporter activity • regulation of fatty acid beta-oxidation • efflux transmembrane transporter activity
EAAT1	• L-glutamate transmembrane transporter activity	ACOX3	• fatty acid beta-oxidation using acyl-CoA oxidase • fatty acid binding
FUCA2	• alpha-L-fucosidase activity • glycoside catabolic process	CAMSAP2	• cytoplasmic microtubule organization • calmodulin binding
HM13	• peptidase activity • aspartic endopeptidase activity	COX6C	• mitochondrial electron transport, cytochrome c to oxygen • generation of precursor metabolites and energy
PTX3	• negative regulation of glycoprotein metabolic process • complement component C1q complex binding	ITGA7	• integrin-mediated signaling pathway • cell adhesion mediated by integrin
RPE65	• phosphatidylserine binding • retinoid metabolic process	NCX1	• calcium:sodium antiporter activity • calcium ion binding • regulation of the force of heart contraction
RPL27A	• structural constituent of ribosome cytoplasmic translation	ROBO1	• Roundabout signaling pathway • aorta development
RPL4	• structural constituent of ribosome cytoplasmic translation	RRP9	• RNA binding • rRNA processing
RPS25	• structural constituent of ribosome cytoplasmic translation		
TOMM40	• protein transmembrane transporter activity • protein targeting to mitochondrion • mitochondrial outer membrane translocase complex		
VMP1	• autophagosome membrane docking • plasma membrane phospholipid scrambling • lipoprotein transport		

Supp. Table S1

compound	concentration	supplier
SNC80	100 μM	Tocris
naltrindole	200 μM	Sigma-Aldrich
DF-TBOA	500 μM	Tocris
aprindine	25 μM (Xenopus) 50 μM (cells)	Santa Cruz
KBR-7943	15 μM (Xenopus) 25 μM (cells)	Sigma-Aldrich
dronedarone	40 μM (Xenopus) 25 μM (cells)	Sigma-Aldrich

Supp. Table S2